



# Millennial hydrological variability in the continental northern Neotropics during Marine Isotope Stages (MISs) 3–2 (59–15 cal ka BP) inferred from sediments of Lake Petén Itzá, Guatemala

Rodrigo Martínez-Abarca<sup>1</sup>, Michelle Abstein<sup>1</sup>, Frederik Schenk<sup>2,3</sup>, David Hodell<sup>4</sup>, Philipp Hoelzmann<sup>5</sup>, Mark Brenner<sup>6</sup>, Steffen Kutterolf<sup>7</sup>, Sergio Cohuo<sup>8</sup>, Laura Macario-González<sup>9</sup>, Mona Stockhecke<sup>10</sup>, Jason Curtis<sup>6</sup>, Flavio S. Anselmetti<sup>11</sup>, Daniel Ariztegui<sup>12</sup>, Thomas Guilderson<sup>13,14</sup>, Alexander Correa-Metrio<sup>15,16</sup>, Thorsten Bauersachs<sup>17</sup>, Liseth Pérez<sup>1</sup>, and Antje Schwalb<sup>1</sup>

<sup>1</sup>Institut für Geosysteme und Bioindikation, Technische Universität Braunschweig, 38106 Braunschweig, Germany

<sup>2</sup>Department of Geological Sciences, Bolin Centre for Climate Research, Stockholm University, 10691 Stockholm, Sweden

<sup>3</sup>Department of Geosciences and Geography, University of Helsinki, 00014 Helsinki, Finland

<sup>4</sup>Godwin Laboratory for Palaeoclimate Research, Department of Earth Sciences, University of Cambridge, Cambridge, CB2 3EQ, UK

<sup>5</sup>Institut für Geographische Wissenschaften, Physische Geographie, Freie Universität Berlin, 12249 Berlin, Germany

<sup>6</sup>Department of Geological Sciences, Land Use and Environmental Change Institute, University of Florida, Gainesville, Florida 32611, USA

<sup>7</sup>GEOMAR Helmholtz Centre for Ocean Research Kiel, 24148 Kiel, Germany

<sup>8</sup>Tecnológico Nacional de México, I. T. de Chetumal, Chetumal, 77013, Mexico

<sup>9</sup>Tecnológico Nacional de México, I. T. de la Zona Maya, Quintana Roo, 77013, Mexico

<sup>10</sup>Large Lakes Observatory (LLO), University of Minnesota Duluth, Duluth, Minnesota 55812, USA

<sup>11</sup>Institute of Geological Sciences, Oeschger Centre for Climate Change Research, University of Bern, 3012 Bern, Switzerland

<sup>12</sup>Department of Earth Sciences, University of Geneva, 1205 Geneva, Switzerland

<sup>13</sup>Center for Accelerator Mass Spectrometry, Lawrence Livermore National Laboratory, Livermore, California 94550, USA

<sup>14</sup>Ocean Sciences Department, University of California, Santa Cruz, Santa Cruz, California 95064, USA

<sup>15</sup>Instituto de Geología, Universidad Nacional Autónoma de México, Mexico City, 04510, Mexico

<sup>16</sup>Centro de Geociencias, Universidad Nacional Autónoma de México, Juriquilla, 76230, Mexico

<sup>17</sup>Institute of Earth Sciences, Heidelberg University, 69120 Heidelberg, Germany

**Correspondence:** Rodrigo Martínez-Abarca (l.martinez-abarca@tu-bs.de)

Received: 12 August 2022 – Discussion started: 26 August 2022

Revised: 24 April 2023 – Accepted: 17 May 2023 – Published: 18 July 2023

**Abstract.** Lake Petén Itzá (Guatemala) possesses one of the longest lacustrine sediment records in the northern Neotropics, which enabled study of paleoclimate variability in the region during the last  $\sim 400\,000$  years. We used geochemical (Ti, Ca/(Ti + Fe) and Mn/Fe) and mineralogical (carbonates, gypsum, quartz, clay) data from sediment core PI-2 to infer past changes in runoff, lake evaporation, organic

matter sources and redox conditions in the water column, caused by hydrological changes in the northern Neotropics during Marine Isotope Stages (MISs) 3–2. From 59 to 39 cal ka BP climate conditions were relatively wet, and the lake was marked by higher primary productivity and anoxic bottom waters. This wet environment was interrupted for two periods of possible low water level at 52 and 46 cal ka BP,

when our data suggest higher evaporation, high terrestrial organic matter input and persistent oxic conditions. Between 39 and 23 cal ka BP, evaporation and input of terrestrial organic matter increased considerably, lake level declined, and lake bottom waters generally became oxic. These conditions reversed during the Last Glacial Maximum (23.5–18.0 cal ka BP), when runoff and lake productivity increased, and rising lake level caused bottom waters to again become anoxic. Comparison of our hydrologic proxy data with sea surface temperature anomalies between the eastern Pacific and the Caribbean suggests that changes in the intensity of the Caribbean Low-Level Jet (CLLJ) may have influenced long-term changes in runoff during MISs 3–2. Higher intensity of the CLLJ during the onset of MIS 3 and the LGM might have led to greater runoff into the lake, whereas the MIS 3–2 transition experienced a weaker CLLJ and consequently less runoff. A refined, high-resolution age–depth model for the PI-2 sediment core enabled us to identify millennial-scale Greenland interstadials (GIs) 14–2, Greenland stadials (GSs) 14–2 and Heinrich stadials (HSs) 5–1. In general, HSs and GSs were characterized by drier conditions. In contrast to GSs and HSs, GIs were characterized by greater runoff and overall wetter conditions, with the most pronounced GI peaks between 40 and 30 cal ka BP. Whereas GSs 9, 8, 7 and 6 began with abrupt increases in evaporation and ended with gradual increases in humidity, GSs 11 and 10 showed reversed patterns. The Lake Petén Itzá paleohydrology record, along with other regional paleoclimate records, led us to conclude that shifts in the position of the Intertropical Convergence Zone (ITCZ) altered moisture delivery to the lake on millennial timescales. During GSs and HSs, high evaporation from Petén Itzá (dry climate conditions) was associated with a more southerly position of the ITCZ, whereas wetter GIs prevailed during a more northerly ITCZ position. Although abrupt millennial-scale shifts in ITCZ and hydroclimate between GSs/HSs and GIs can be linked to instabilities in the Atlantic Meridional Overturning Circulation (AMOC), longer-term changes were additionally influenced by changes in atmospheric convection linked to modulations of the CLLJ in response to  $\Delta$ SST between the equatorial Pacific and tropical Atlantic.

## 1 Introduction

The last glacial period (115–11.7 cal ka BP) was marked by strong millennial-scale climate variability in the high-latitude Northern Hemisphere. Marine Isotope Stage (MIS) 3 (59–29 cal ka BP) and the last deglaciation (18–11.7 cal ka BP) were dominated by abrupt climate events (e.g., Heinrich, 1988; Lisiecki and Stern, 2016; Bradley and Diaz, 2021). In the Greenland ice core, these are referred to as Dansgaard–Oeschger (D–O) events (Johnsen et al., 1992) and consist of rapid oscillations between cold Greenland stadials (GSs) and

warm Greenland interstadials (GIs). During some of the most extreme GSs, North Atlantic marine sediment cores were found to contain layers of ice-rafted debris (IRD) rich in detrital carbonate derived from Paleozoic bedrock that underlies the Hudson Strait (Heinrich, 1988; Broecker et al., 1992; Hemming, 2004). These so-called “Heinrich events” (Heinrich, 1988; Broecker et al., 1992) were attributed to massive discharges of icebergs from the Laurentide Ice Sheet to the North Atlantic via the Hudson Strait and in some cases to a European origin (e.g., Grousset et al., 2000). GSs that contain Heinrich events are referred to as Heinrich stadials (HSs). Freshwater forcing associated with Heinrich events weakened the Atlantic Meridional Overturning Circulation (AMOC), and the Intertropical Convergence Zone (ITCZ) moved south, resulting in periods of abrupt, substantial rainfall changes in the tropics and subtropics, referred to as “tropical hydroclimate events” (Bradley and Diaz, 2021). Paleoclimate records from the northern Neotropics revealed that during those events, cool and dry conditions prevailed. For instance, such conditions were recorded in a speleothem record from Cuba by a reduction in growth rates and higher  $\delta^{18}\text{O}$  values (Warren et al., 2019).

Lake Petén Itzá, northern Guatemala (Fig. 1), is located in a geologically and biologically diverse region that is climatically sensitive (Macario-González et al., 2022), affected by the annual migration of the ITCZ, trade wind intensity and moisture transport from the Caribbean Sea. The lake sediments represent one of the longest ( $\sim 400$  kyr) paleoclimate archives in the Neotropics (Kutterolf et al., 2016). Few paleoclimate records from the northern Neotropics are older than 100 kyr in age (e.g., Lake Chalco, central Mexico; Martínez-Abarca et al., 2021a). In addition, the relatively high sedimentation rate in Lake Petén Itzá enables high-temporal-resolution sampling, making it possible to investigate abrupt, short-duration climate changes such as GS and GI events during MISs 3–2. This has been possible only for a few paleoclimate records from the Caribbean and the Gulf of Mexico region (e.g., Warren et al., 2020a). For example, the Mg/Ca record from a speleothem in Cuba (Santo Domingo Cave) documented relatively humid conditions during GIs and drier climate during GSs (Warren et al., 2019). GSs were identified in earlier studies of Lake Petén Itzá sediments and suggested that mean annual air temperature (MAAT) was 19–20 °C, 6 °C lower than the modern annual atmospheric temperature in the lowland northern Neotropics (Correa-Metrio et al., 2012). The cooler conditions were accompanied by high fire frequency around the lake (Correa-Metrio et al., 2012). Identification of dry conditions during HSs was initially based on the presence of gypsum layers (Hodell et al., 2008; Mueller et al., 2010). Subsequent work suggested an even greater decline in MAAT in the region during HSs, between 6 and 10 °C (Hodell et al., 2012; Grauel et al., 2016). Evidence from an ostracod transfer function suggested Lake Petén Itzá experienced a decline in mean water temperature of 3 °C during HSs (Cohuo et al., 2018; Pérez et al., 2021). In

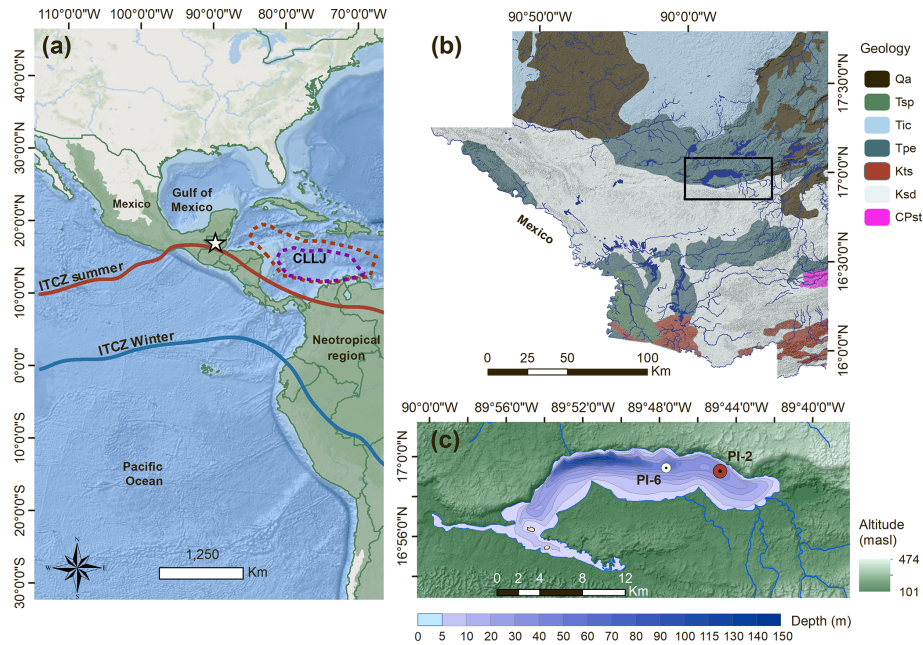


**Figure 1.** Location of Lake Petén Itzá, along with regional climatological and geological information. **(a)** Location of Guatemala in Central America and geographic position of the lake (white star). Neotropical region (green; shapefile obtained from Löwenberg-Neto, 2014) and ITCZ positions during summer (red) and winter (purple). The extent of the CLLJ in summer (red) and winter (purple) is shown. The dashed lines represent the zonal easterly winds greater than  $16 \text{ m s}^{-1}$  at 925 mbar level associated with the CLLJ. Service layer credits: Esri, Garmin, GEBCO, NOAA and NGDC (World Topography and Oceans Maps; Esri Canada Education and Research Group; under CC BY-NC license, 2022; scale not given). **(b)** Overview of geology in northern Guatemala and location of Lake Petén Itzá (black rectangle) region: Qa – Quaternary alluvium, Tsp – Tertiary upper Oligocene–Pliocene, Tic – Eocene sedimentary rocks, Tpe – Paleocene–Eocene marine sediments, Kts – Cretaceous–Tertiary clastic sediments, Ksd – Cretaceous carbonaceous rocks, CPst – Carboniferous–Permian sand conglomerate (geological information: IGN, 1970). **(c)** Digital elevation model, principal rivers and streams, and bathymetry of Lake Petén Itzá; location of core sites: PI-2 (red dot) and PI-6 (white dot).

addition, stable-oxygen-isotope measures on ostracod shells revealed a relatively greater evaporation / precipitation ratio during HSs, from which lower lake levels and drier climate conditions were inferred (Escobar et al., 2012). During HS 1 (18–15 cal ka BP), which followed the Last Glacial Maximum (23–18 cal ka BP) and is one of the most studied periods in the Petén Itzá record, the presence of nektonic ostracod species such as *Cypridopsis vidua* and *Cypria petenensis* (previously called *C. okeechobei* and *Physocypria globula*), as well as the appearance of *Paracythereis opesta* (previously called *Limnocythere opesta*), suggests a relatively cold lake with high primary productivity and lower water levels (Pérez et al., 2013). These cold and dry conditions promoted the establishment of savanna vegetation dominated by Poaceae and *Acacia*, and in the lake, littoral “colder-water” ostracod species such as *Cytheridella ilosvayi* and *Paracythereis opesta* were abundant (Pérez et al., 2021).

Previous paleoclimate and paleoenvironmental information about MISs 3–2 was obtained primarily from Site PI-6 (water depth 71 m), one of the seven sites drilled in Lake Petén Itzá. Site PI-2, where the water depth is 54 m, is located 3 km east of Site PI-6 and showed a higher mean long-term sedimentation rate ( $\sim 150 \text{ cm kyr}^{-1}$  (Site PI-2) vs.  $\sim$

$117 \text{ cm kyr}^{-1}$  (Site PI-6); Kutterolf et al., 2016). Therefore, millennial paleoclimate information was recorded at greater temporal resolution at Site PI-2, though the record covers a shorter time span ( $\sim 59 \text{ kyr}$ ). Another advantage of Site PI-2 is that it lies in a flatter area and is thus less affected by episodic slumping that influences sedimentation rate. For this study, we used high-resolution geochemical and mineralogical data from Site PI-2 sediments to explore hydrological variability in the northern Neotropics during MISs 3–2 (59–15 cal ka BP). We compared our results from Lake Petén Itzá with other regional records to better understand potential impacts and drivers of climate changes, particularly mechanisms that caused shifts in moisture transport to the northern Neotropics.

## 2 Study area

### 2.1 Location and climate

Lake Petén Itzá is located in the northern lowlands of Petén, northern Guatemala ( $16^{\circ}59'39.90'' \text{ N}$ ,  $89^{\circ}49'21.07'' \text{ W}$ ; 110 m a.s.l. – above sea level; Fig. 1). It has a surface area of  $\sim 100 \text{ km}^2$  and a maximum depth of 165 m (Hodell

et al., 2006). The region has a humid tropical climate (“Af” according to the Köppen classification), with mean monthly air temperatures ranging from 22 to 30 °C (INSIVUMEH, 2021). Mean annual precipitation is  $\sim 1600$  mm (INSIVUMEH, 2021) but varies intra-annually, with a pronounced dry season from January to May and a wet season that extends from late May through December. The climate of the northern Neotropics, particularly in terms of precipitation, is influenced by different climate forcing mechanisms that are still debated. First, the rainy season is during the summer, when the ITCZ is in its northernmost position. Second, the Caribbean Low-Level Jet (CLLJ), a region of maximum horizontal wind speeds (up to  $16 \text{ m s}^{-1}$ ) at 925 mbar level, is linked to a precipitation maximum along the Caribbean and Central American coasts mainly between June and July (Amador et al., 2000). The CLLJ is a complex system that responds to large-scale atmospheric changes, the Atlantic Warm Pool, and topographic effects and land–sea contrast in addition to variations in the sea surface temperature (SST) gradient between the eastern equatorial Pacific Ocean and Caribbean Sea (Spence et al., 2004; Wang, 2007). When the Pacific has higher temperatures than the Atlantic, the CLLJ intensifies towards the northern Caribbean, and consequently, precipitation increases in Petén (Whyte et al., 2008). Humidity can also be transported by the North American Monsoon (NAM) towards the north of Mexico from the Gulf of Mexico and the Caribbean, mainly during July and September, when atmospheric temperatures reach their maximum, and the monsoon migrates northward (Hu and Dominguez, 2015).

## 2.2 Geology

Lake Petén Itzá lies in a basin formed by asymmetric faulting (Fig. 1). To the north are marine carbonates of Paleocene–Eocene age, whereas to the south, surface rocks are composed of Cretaceous limestones (IGN, 1970). To the southeast, Quaternary alluvial sediments, rocks and soils dominate, the latter consisting mainly of carbonates and clays (Simmons et al., 1959; IGN, 1970; Mueller, 2009). The karst geology of the region promotes rapid infiltration of rainfall into the groundwater (Hodell et al., 2008), although a slow-flowing ephemeral stream at the southeastern end of Lake Petén Itzá transports water and sediment into the lake during the rainy season.

## 3 Methods

### 3.1 International Continental Scientific Drilling Program (ICDP) drilling campaign

During February and March 2006, multiple cores were drilled at seven locations in Lake Petén Itzá (PI-1, PI-2, PI-3, PI-4, PI-6, PI-7 and PI-9) as part of an International Continental Scientific Drilling Program (ICDP) project (Petén

Itzá Scientific Drilling Program, PISDP). Maximum drilling depth, 133 m, was achieved at Site PI-7. Sedimentology, magnetic susceptibility and density data for the cores were presented by Hodell et al. (2006, 2008) and Mueller et al. (2010). Here, we focus on the sediment sequence recovered from Site PI-2. The site displayed a relatively high mean sedimentation rate ( $\sim 150 \text{ cm kyr}^{-1}$ ; Kutterolf et al., 2016) and an average core recovery of 86.3 %, which enabled climate and environmental studies at high temporal resolution. The PI-2 sequence was retrieved from a water depth of 54 m in the eastern part of the lake ( $16^{\circ}59'58.04'' \text{ N}$ ,  $89^{\circ}44'41.51'' \text{ W}$ ; Fig. 1c). The drill site receives detrital material in the form of colluvium from the steep northern shore. Five holes were drilled at Site PI-2, the longest of which reached a sediment depth of  $\sim 67$  m. The composite sequence at Site PI-2 was divided into 11 lithostratigraphic units based on changes in facies composition (Mueller et al., 2010). For this study, we analyzed sediment samples from Units 6 to 2 (67–19 m depth), which span the interval of MIS 3–2 (Correa-Metrio et al., 2012; Escobar et al., 2012).

### 3.2 Age–depth model

Previous studies used slightly different chronologies for the sediment sequences from Lake Petén Itzá, with a focus on the composite section from Site PI-6. Those studies used linear interpolation between radiocarbon dates (Hodell et al., 2008; Mueller et al., 2010), projection onto the PI-6 sequence of accelerator mass spectrometry (AMS)  $^{14}\text{C}$  dates from other cores (Escobar et al., 2012) and ages of tephra layers (Kutterolf et al., 2016). Mays et al. (2017) constructed a Bayesian age model for Site PI-6. We similarly refined the age–depth model for PI-2 using a Bayesian model (Blaauw and Christen, 2011). In this model (PETEN 02), we used 20 radiocarbon ages from the PI-2 sequence that were reported by Mueller et al. (2010) and Escobar et al. (2012), together with four dated tephra layers identified in the PI-2 core (Kutterolf et al., 2016; Table 1). Radiocarbon ages were calibrated using the IntCal20 curve (Reimer et al., 2020). The model was established using the Bacon package (Blaauw and Christen, 2011) of the RStudio software (v. 4.2). An initial estimated mean sedimentation rate of  $1 \text{ mm yr}^{-1}$  ( $100 \text{ cm kyr}^{-1}$ ) for 28 segments along the core was determined. Processes that deposit material rapidly at the bottom of the lake, such as turbidite flows and volcanic ashfalls, can confound the chronology by contributing substantial amounts of material in a short time span (Moernaut et al., 2017; Mulder et al., 2019). Hence, we excluded 31 such deposits during age modeling, including carbonaceous turbidites and tephra layers, identified using the descriptions of Mueller et al. (2010; Appendix A).

**Table 1.** AMS  $^{14}\text{C}$  dates and ages of tephra used for the age–depth model. Data with <sup>a</sup> are measurements of terrestrial organic matter (i.e., woody debris; Mueller et al., 2010). Sample lab IDs with <sup>b</sup> are tephra layers (Kutterolf et al., 2016). All radiocarbon dates were calibrated using a Bayesian model (Blaauw and Christen, 2011) and the IntCal20 curve (Reimer et al., 2020); “avg” in the lab ID column refers to the mean age obtained from two dates on the same sample.

Lab ID	Core, section (cm)	Depth (m)	Age ( $^{14}\text{C}$ yr)	$\pm(1\sigma)$	Mean (cal yr BP)	Modeled age range (cal yr BP)
144277 <sup>a</sup>	2D-1H-1, 14	0.22	425	30	22	–60–150
139341 <sup>a</sup>	2D-2H-2, 25	4.88	1715	35	1620	1516–1737
139342_avg <sup>a</sup>	2B-4H-2, 39	10.25	3740	33	4043	3655–4169
144270 <sup>a</sup>	2A-5H-1, 87	10.85	4280	30	5203	4903–5288
139344_avg <sup>a</sup>	2B-5H-1, 102	12.45	7468	40	8276	8170–8390
139346 <sup>a</sup>	2D-5H-1, 56	12.76	7835	30	8736	8614–8875
139399 <sup>a</sup>	2B-6H-2, 41	16.43	11 135	40	13 057	12 909–13 168
139399 <sup>a</sup>	2D-6H-2, 44	17.46	11 880	35	13 637	13 439–13 792
144272 <sup>a</sup>	2A-8H-1,96	20.44	13 095	40	15 710	15 497–15 907
139400 <sup>a</sup>	2D-8H-1, 5	21.65	13 480	45	16 197	16 059–16 326
139401_avg <sup>a</sup>	2B-8H-1, 132	22.24	13 533	45	16 408	16 225–16 600
139402 <sup>a</sup>	2B-9H-1, 146	25.47	15 355	50	18 632	18 321–18 820
144274 <sup>a</sup>	2B-10H-2, 98	29.59	19 740	70	23 904	23 535–24 236
144269 <sup>a</sup>	2A-12H-1, 47	31.49	21 940	80	26 176	25 932–26 661
139403 <sup>a</sup>	2B-12H-1, 121	38.41	25 540	160	35 488	32 614–37 722
139404 <sup>a</sup>	2A-14H-1, 115	40.38	32 680	980	36 947	34 181–38 962
139405 <sup>a</sup>	2A-16H-1, 66	44.55	34 380	450	39 794	38 469–40 926
139406 <sup>a</sup>	2C-2H-1, 135	47.08	38 760	740	42 621	41 955–43 422
139407 <sup>a</sup>	2A-17H-1, 104	48.06	41 350	1020	43 944	42 974–44 960
139343 <sup>a</sup>	2A-17H-1, 151	48.4	41 600	900	44 195	43 186–45 263
C1 <sup>b</sup>	2B-5H-2, 65	13.09	9805	100	9378	9231–9550
C2 <sup>b</sup>	2A-7H-1, 131	17.69	13 158	100	13 761	13 537–13 959
C4 <sup>b</sup>	2A-19H-2, 10	54.46	49 100	2000	48 793	45 957–52 137
C5 <sup>b</sup>	2C-9E-1, 114	64.22	53 000	3000	55 826	51 080–62 132

### 3.3 X-ray fluorescence sediment analysis

X-ray fluorescence (XRF) measurements were carried out at the University of Minnesota, Duluth, using a Cox Analytical Itrax Core Scanner (Cr tube, 30 kV, 55 mA, 15 s exposure) with a resolution of 1 cm. Particular focus was given to titanium (Ti), aluminum (Al), calcium (Ca), iron (Fe) and manganese (Mn) because these elements are reliable indicators of runoff (Ti, Al), evaporation (Ca) and redox conditions (Fe, Mn). Data from XRF, in counts per second (cps), were processed using a centered log ratio (CLR) transformation, following Weltje et al. (2015). CLR-transformed compositional data express elemental quantities in terms of actual concentrations and incorporate uncertainties acquired during core scanning, such as sediment water content, grain size and irregularities of the sediment surface (Dunlea et al., 2020). For each XRF measurement, we divided an element (e.g.,  $\text{Ti}_{(\text{cps})}$ ) by the geometric average of the geochemical set (Ti, Al, Ca, Fe and Mn). The natural logarithm of the ratio was then calculated (e.g.,  $\ln(\text{Ti}_{(\text{cps})}/\text{geometric average})$ ). Calibration was carried out using Xelerate software (Bloemsma, 2015; Weltje et al., 2015). A principal component analysis (PCA) was carried out with CLR data (Appendix B) to distinguish

the processes that control each element. The PCA results are given in Appendix B. We used these results to define the  $\text{Ca}/(\text{Ti} + \text{Fe})$  ratio as an indicator of evaporation and the  $\text{Mn}/\text{Fe}$  as a proxy for redox processes (Wersin et al., 1991; Yarincik et al., 2000). Simultaneously, a LOESS smoothing function was applied to the CLR data to dampen the noise signal from measurement errors or anomalous data. LOESS smoothing was carried out in RStudio (v. 4.2) (R Core Team, 2018) with a span value of 3.

### 3.4 X-ray diffraction for sediment mineral analysis

To document changes in sediment mineralogy, 100 samples from Site PI-2 cores were used for X-ray diffraction (XRD) analysis. Sampling was carried out at irregular intervals ranging from 0.5 to 1.0 m. Sediment samples were dried at room temperature and ground with a mortar and pestle. Measurements were conducted with a Rigaku MiniFlex 600 (15 mA/40 kV) XRD at the Department of Physical Geography, Freie Universität Berlin. Peaks obtained from 3 to 80° of rotation were identified with X-Pert High Score (Version 1.0b) from Philips Analytical. The peaks were calibrated against the main quartz

peak (I100) at  $d = 0.334$  nm (3.34 Å). Diffraction potential files of the International Centre for Diffraction Data, USA, were used as references for identification of the different mineral phases. The quartz and gypsum counts, the sum of montmorillonite + vermiculite (clay) and the sum of calcite + dolomite + aragonite + magnesium calcite (carbonate) were added, and the relative percentages were calculated as follows: mineral (%) = (mineral count · 100) /  $\Sigma$  minerals (Last, 2001).

### 3.5 Geochemistry of bulk sediment

Analyses of total carbon (TC), total organic carbon (TOC), total inorganic carbon (TIC) and total nitrogen (TN) were carried out on the same sediment samples used for XRD. All measurements were performed at the Department of Geological Sciences, University of Florida, Gainesville. TC and TN were determined with a Carlo Erba NA1500 CNS elemental analyzer. TIC was measured coulometrically (Engleman et al., 1985) with a UIC CO<sub>2</sub> coulometer 5011 (Coulometrics) coupled with an AutoMate preparation device. TOC was calculated as the difference between TC and TIC. TOC/TN ratios are reported on a molar basis.

## 4 Results

### 4.1 Chronology

Data presented in this study cover the depth interval from 67 to 19 m in the PI-2 record, corresponding to an age range from 59 to 15 cal ka BP (Fig. 2). From the sediment surface to 51 m depth, average age uncertainty is  $\pm 0.8$  kyr. The uncertainty in the chronology increases in the deeper sediment intervals, especially below 51 m depth ( $> 46$  cal ka BP), resulting in  $\pm 6.7$  kyr at the bottom of the sequence (67 m sediment depth). There were two intervals during which event deposits (mainly carbonaceous turbidites) were abundant: between 67 and 48 m sediment depth (58.5–43.8 cal ka BP) and from 23 to 19 m (16.6–15.0 cal ka BP). Our age–depth model differs from the one of Kutterolf et al. (2016), mainly in the interval between 40 and 34 cal ka BP, where ages calculated by our model are as much as 2 kyr younger. This is, however, within the average uncertainty in our age model at these depths (greater than  $\pm 2.3$  kyr).

### 4.2 Climate proxies

Results are presented by age and according to the lithostratigraphic units proposed by Mueller et al. (2010; Fig. 3; Appendix B). CLR values for Ti vary between  $-2.1$  (low runoff) and  $+1.6$  (high runoff) throughout the sequence, with an average of  $-0.1 \pm 0.3$  (Fig. 3). In Units 6 and 5, Ti is characterized by fluctuating values that range between  $-1.6$  and  $+0.7$ . The lowest average values ( $\leq -2.1$ ) were observed in

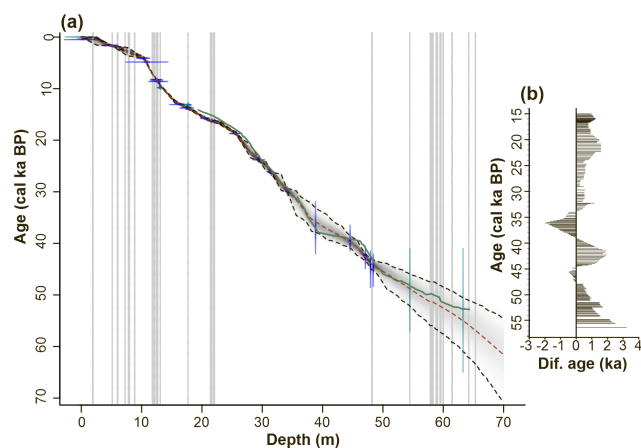


**Figure 2.** Age–depth model for the PI-2 record: (a) chronology of the PI-2 record. Gray vertical lines indicate the location of the 32 instantaneous deposits that were removed for the modeling. Ages and their uncertainties are indicated in blue. The solid green line shows the chronology obtained by Kutterolf et al. (2016) and used by Cohuo et al. (2018, 2020). The dashed red line represents the average age, whereas the dashed black lines are the minimum and maximum range for each age. (b) Age difference between the model used in this study and the one presented by Kutterolf et al. (2016) in the interval between 59 and 15 cal ka BP. Data were calculated as follows: age difference (ka) = age of this study – age reported by Kutterolf et al. (2016).

Unit 4. Units 3 and 2 display the highest Ti content, both with maxima of  $+1.1$ .

CLR values of Ca/(Ti + Fe) range from  $-0.1$  (low evaporation) to  $+6.4$  (high evaporation) throughout the sequence, with an average of  $+3.0 \pm 1.0$  (Fig. 3). In Units 6 and 5, Ca/(Ti + Fe) is variable ( $+0.7$  to  $+5.9$ ), with a mean of  $+2.8 \pm 0.8$  and three pronounced peaks of  $+5.2$  (51.9 cal ka BP, 58.9 m),  $+5.8$  (46.1 cal ka BP, 50.8 m) and  $+5.4$  (40.3 cal ka BP, 45.3 m). The ratio increases in Unit 4 and ranges from  $+1.5$  to  $+5.9$  (mean =  $+3.6 \pm 0.7$ ). Unit 3 displays the lowest Ca/(Ti + Fe), varying between  $-0.1$  and  $+4.0$  (mean =  $+1.9 \pm 0.5$ ). Unit 2 is characterized by highly variable Ca/(Ti + Fe), ranging between  $-0.1$  and  $+6.4$  (mean =  $+3.3 \pm 1.4$ ), and shows the highest values of up to  $+6.4$  at the top of the interval.

CLR values of Mn/Fe ratios range between  $-7.4$  (anoxic) and  $+0.2$  (oxic), with an average of  $-3.4 \pm 0.6$  throughout the record (Fig. 3). Unit 6 displays the lowest values of the sequence, ranging from  $-6.6$  to  $-2.7$ . Unit 5 presents a gradual increase in Mn/Fe ratios between 52.7 and 46.1 cal ka BP (60.0–50.8 m), reaching as high as  $-1.1$ . Units 5 and 4 show similar values, which vary from  $-7.4$  to  $+0.2$ , with maxima of  $+0.2$  (46.2 cal ka BP, 50.8 m),  $-1.6$  (40.2 cal ka BP, 45.3 m),  $-1.7$  (37.1 cal ka BP, 40.5 m) and  $-0.8$  (29.6 cal ka BP, 34.3 m). In Units 3 and 2 values fluctuate between  $-7.3$  and  $-2.6$  (mean =  $-3.8 \pm 0.5$ ).

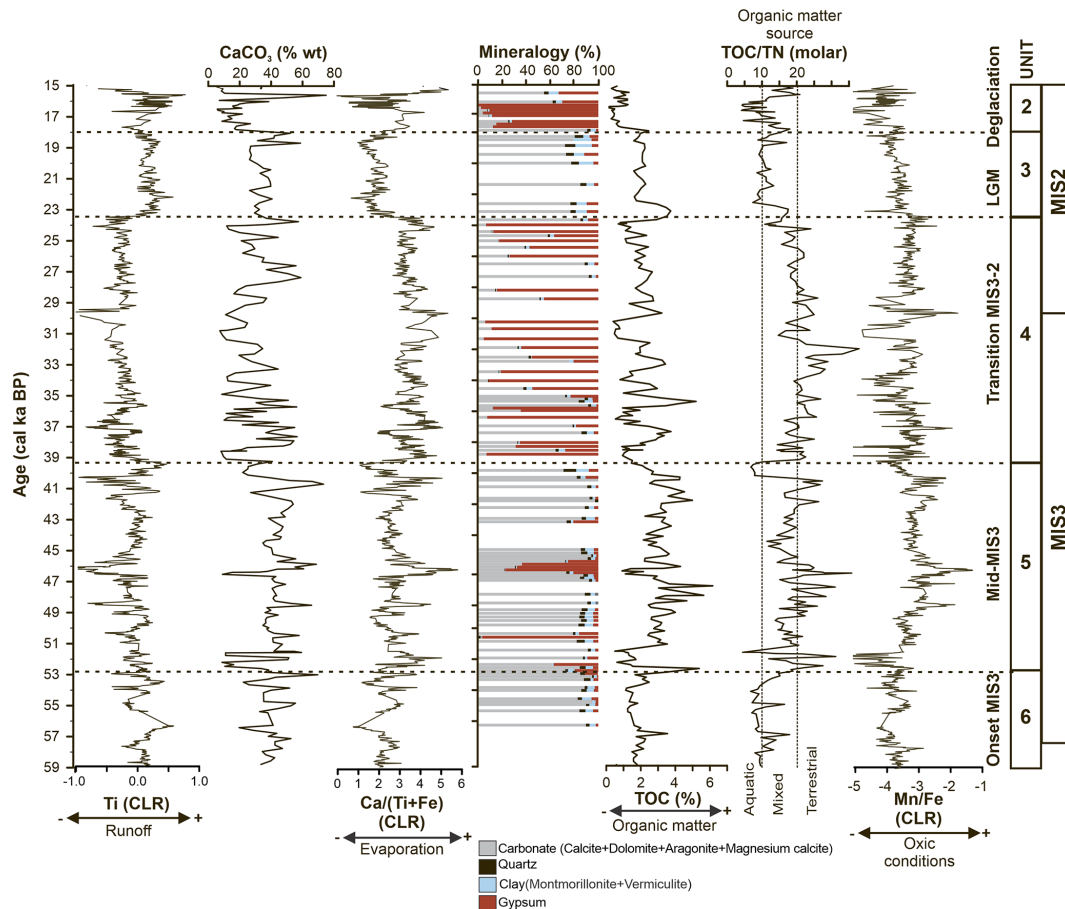


**Figure 3.** Sediment variables in the PI-2 sequence, between 59 and 15 cal ka BP. Horizontal dashed black lines indicate periods that coincide with unit boundaries described by Mueller et al. (2010). The timing of the MIS 3–2 transition and the Last Glacial Maximum (LGM) is shown on the right (Lisiecki and Raymo, 2005). Runoff and evaporation are indicated by Ti centered log ratio (CLR) values and Ca/(Ti + Fe) ratios, respectively. Carbonate (CaCO<sub>3</sub>) content is shown as percentage dry weight (% wt). Percentages of quartz, clay (montmorillonite + vermiculite) and gypsum are shown. Total organic carbon is an indicator of primary productivity, ratios of total organic carbon to total nitrogen (TOC/TN) are indicators of organic matter sources, and the CLR value of Mn/Fe is used as a proxy for redox conditions.

The mineralogical composition of the Lake Petén Itzá record, determined by XRD, is dominated by carbonates, including calcite, dolomite, aragonite and magnesium calcite. About 65 % of the sediment samples contained more than 50 % carbonate, with calcite (mean  $45.9 \pm 2.7$  %) and dolomite (mean  $13.4 \pm 1.3$  %) being most common. Quartz shows the highest average values in Units 6 ( $3.0 \pm 1.5$  %), 5 ( $3.2 \pm 2.0$  %) and 3 ( $5.1 \pm 2.5$  %). The clay content (montmorillonite + vermiculite) is highly variable throughout the record, ranging from 0 % to 13.7 % (mean  $3.6 \pm 3.0$  %). It shows a gradual decrease from Unit 6 (4.5 %) to Unit 4 (2.1 %). Unit 3 contains the highest clay content (mean  $8.5 \pm 2.9$  %) but decreases upward to an average of 1.9 % in Unit 2. The gypsum content is highly variable and ranges from 0 % to 100 %, with an average of  $32.6 \pm 3.6$  % (Fig. 3). Units 6, 5 and 3 show the lowest gypsum content of the record, with average values of 5.1 %, 14.9 % and 6.2 %, re-

spectively. In Unit 5, maxima of 96.8 % and 77.7 % occur at 50.9 cal ka BP (56.8 m) and 46.3 cal ka BP (51.1 m), respectively. In Units 4 and 2, a large increase in gypsum content is observed, with average values of 53.9 % and 78.2 %, respectively.

CaCO<sub>3</sub> values obtained by XRD vary from 4.2 % to 75.0 %, with an average of  $33.9 \pm 15.3$  %. Units 6 and 5 show similar values of CaCO<sub>3</sub>, oscillating between 8.7 % and 73.4 % (mean  $40.7 \pm 12.4$  %). A reduction in the CaCO<sub>3</sub> content characterizes Unit 4, with an average of  $28.9 \pm 14.9$  %. In Unit 3, concentration values vary from 26.3 % to 58.7 % (mean =  $34.7 \pm 7.5$  %). Unit 2, with an average of  $20.9 \pm 17.9$  %, is characterized by a slight decrease in CaCO<sub>3</sub> content but shows a maximum of 75.0 % at 15.5 cal ka BP.

TOC values vary between 0.2 % and 6.1 %, with an average of  $2.1 \pm 1.1$  % throughout the sequence (Fig. 3). In Unit 6, TOC values range from 1.1 % to 4.5 %. Unit 5 dis-

plays TOC values that range from 0.5 % to 6.1 % and decrease substantially around 47.2 cal ka BP (52.3 m). From 37.8 to 30.9 cal ka BP (42.0 to 35.0 m) in Unit 4, there are three distinct maxima, with TOC values of 3.7 % (37.3 cal ka BP, 41.1 m), 5.2 % (35.4 cal ka BP, 38.4 m) and 3.4 % (33.0 cal ka BP, 36.5 m). The TOC content in Unit 3 increases to a maximum of 3.7 %, with an average of  $2.2 \pm 0.6$  %. Unit 2 is characterized by lower TOC values, which vary from 0.2 % to 2.5 % (mean  $0.7 \pm 0.4$  %).

Molar TOC/TN ratios range from 4 (high aquatic-organic-matter content) to 38 (high terrestrial-organic-matter content) throughout the record (mean  $16.8 \pm 6.3$ ). Unit 6 shows TOC/TN ratios that average  $10.7 \pm 3.2$ , with a gradual increase to 18.9 at the top of the unit (Fig. 3). Units 5 and 4 display similar TOC/TN ratios, ranging between 4.4 and 38. Four maxima of 31.3 (51.8 cal ka BP, 58.6 m), 35.9 (46.4 cal ka BP, 51.0 m), 27.4 (40.4 cal ka BP, 45.3 m) and 38 (31.9 cal ka BP, 35.7 m) were identified, as were minima of  $\sim 6.8$  between 40.3 and 39.2 cal ka BP (45.2–43.9 m depth). At the top of Unit 4 (31.0–23.4 cal ka BP, 35.0–29.0 m depth), TOC/TN ratios decrease gradually from 26.1 to 10.8. Units 3 and 2 have the lowest values of the entire sequence, ranging between 4.6 and 17.5, with a slight increase to 20.9 at the top of Unit 2.

## 5 Discussion

Discussion of the Lake Petén Itzá paleoenvironment focuses on three key objectives: (1) hydrological variability during MISs 3–2 and millennial oscillations (GSs, GIs and HSs) recorded at Site PI-2, (2) comparison of our Site PI-2 data with previously reported data from Site PI-6, and (3) identification of climate forcing mechanisms that may have provided humidity to the Petén area through trans-regional proxy comparison. Our mineralogical and geochemical data are presented and interpreted according to the five periods that correspond to Lithological Units 6–2 proposed by Mueller et al. (2010) (Appendix C): (a) onset of MIS 3 (Unit 6: 59–52.7 cal ka BP), (b) mid-MIS 3 (Unit 5: 52.7–39.3 cal ka BP), (c) MIS 3–2 transition (Unit 4: 39.3–23.5 cal ka BP), (d) Last Glacial Maximum (Unit 3: 23.5–18.0 cal ka BP) and (e) deglaciation (Unit 2: 18.0–15.0 cal ka BP). The lithological units were based on sedimentology and stratigraphy and verified with core-logging data (density, magnetic susceptibility) and with seismic reflection profiles throughout Lake Petén Itzá basin.

### 5.1 Hydrological and environmental responses during MISs 3–2

#### 5.1.1 Onset of MIS 3 (59–52.7 cal ka BP): high runoff and low evaporation

The onset of MIS 3 corresponds to Unit 6. Ti is widely used as an indicator for runoff (Mason and Moore, 1982; Davies

et al., 2015). High Ti (up to 0.7) in this unit suggests high runoff, particularly around 56 cal ka BP (Fig. 3). This is supported by concomitantly high clay and quartz content, with averages of 4.5 % and 3.0 %, respectively. Clay minerals, particularly montmorillonite and vermiculite, are generated during chemical weathering of unstable siliciclastic minerals such as plagioclase, especially in tropical regions where atmospheric humidity is high, resulting in the enrichment of quartz (Weltje, 1994; Boggs, 2006; Van De Kamp, 2010). Quaternary alluvial sediments could be the source of siliciclastic minerals (Simmons et al., 1959; Mueller, 2009). We suggest that the high clay and quartz content in Unit 6 is indicative of wet conditions, which provided abundant runoff to the lake.

Ca provides information on supersaturation and precipitation of ions in solution, triggered by high evaporation (Engstrom and Wright, 1984; Boyle, 2001). Ca in lake sediments, however, can also originate from detrital inputs in karst regions such as in Petén and from biogenic sources, e.g., shell formation by mollusks and ostracods and CO<sub>2</sub> withdrawal by plants for photosynthesis. Therefore, we normalized Ca values to indicators of detrital input such as Ti and Fe (Appendix B) and used the Ca/(Ti + Fe) as an indicator for past variability in evaporation (Mason and Moore, 1982; Yarincik et al., 2000). Low Ca/(Ti + Fe) ratios (mean  $2.3 \pm 0.6$ ) and gypsum content (mean  $5.0 \pm 5.1$  %) at the onset of MIS 3 indicate low evaporation of lake water and more humid conditions, with only a few intermittent dry periods, at  $\sim 55.1$  and 53.8 cal ka BP (Fig. 3).

The TOC/TN ratio has long been used as an indicator for the source of organic matter in lacustrine sediment sequences (Talbot and Johannessen, 1992; Meyers and Ishiwatari, 1995). In the interval between 59 and 53 cal ka BP, low TOC/TN ratios (mean  $10.7 \pm 3.2$ ) indicate that the sediment organic matter is predominantly of aquatic origin (Meyers, 2003). The Mn/Fe ratio is used to infer variations in redox conditions in lakes (Wersin et al., 1991; Naehrer et al., 2013; Friedrich et al., 2014; Ortega-Guerrero et al., 2020). Lower values of the Mn/Fe ratio generally indicate low concentration of O<sub>2</sub> in the water column, which is explained by more rapid reduction in Mn compared to Fe under anoxic conditions, favoring preferential Mn deposition. In contrast, higher values of the Mn/Fe ratio suggest high levels of O<sub>2</sub>, as Fe oxidizes faster than Mn in oxic environments. Low Mn/Fe ratios (mean  $-3.7 \pm 0.3$ ) indicate anoxic conditions in the lake's bottom waters. Anoxia may have been associated with a high water level (as is observed today), which likely prevented wind-driven mixing of the entire water column.

High values of magnetic susceptibility measured at Site PI-6 (Fig. 4) support our interpretation of a wet climate, compared to the less humid environment inferred for the end of MIS 3 (48–23 cal ka BP; Hodell et al., 2008). Previously reported ostracod data from Sites PI-2 (Cohuo et al., 2020) and PI-6 (Pérez et al., 2021) are consistent with substantial precipitation in the study area during the deposition of Unit 6

and are associated with high water levels, reflected by the dominance of *Cypria petenensis*. Moreover, the low content of terrestrial organic matter at Site PI-2 is consistent with the pollen-based inference for extensive grasslands around Lake Petén Itzá, indicating relatively little terrestrial plant biomass in the watershed (Bush et al., 2009; Fig. 4).

Predominantly wet conditions during the onset of MIS 3, like those inferred from Lake Petén Itzá sediments, have also been reported from other sites in the northern Neotropics (Fig. 5) using geochemical records. They include lakes Chalco, central Mexico (Martínez-Abarca et al., 2021b) and Babicora, northern Mexico (Roy et al., 2013). In contrast, pollen and sedimentological information from Lake Fúquene (Colombia) indicates moderately dry conditions and a reduction in lake surface area associated with a decline in precipitation in northern South America (Groot et al., 2013). Differences in precipitation between the northern and southern limits of the American tropics were likely associated with the latitudinal position of the ITCZ (Jaeschke et al., 2007; Gibson and Peterson, 2014; Martínez-Abarca et al., 2021b; Lozano-García et al., 2022).

Reflectance data from marine sediments collected in the Cariaco Basin, Venezuela (Deplazes et al., 2013a), and  $\delta^{18}\text{O}$  data from marine record MD02-2529 retrieved from the eastern equatorial Pacific (Leduc et al., 2007a) indicate a more northerly position of the ITCZ during the onset of MIS 3. Hodell et al. (2008) suggested that increases in runoff in Petén Itzá co-occurred with increases in SST in the subtropical northeast Atlantic (Site SU8118, Portugal; Bard et al., 2000). SSTs between sites in the region, however, have not yet been considered. Therefore, we compared the Ti data from Site PI-2 with the SST difference ( $\Delta\text{SST}$ ) calculated between Site MD02-2529 in the eastern Pacific (Leduc et al., 2007a) and ODP Site 999A in the Caribbean (Schmidt et al., 2006a; Fig. 6). It should be noted though that  $\Delta\text{SST}$  yields considerable uncertainties associated with the prediction error of the quantitative estimation of SST in both records, their age–depth models and the calculation of  $\Delta$  itself because of the use of different temperature proxies (Mg/Ca planktonic foraminifera for ODP-999A and alkenone  $U^{K}_{37}$  for MD02-2529) and temporal resolutions. Even with these limitations, the  $\Delta\text{SST}$  record, used as a CLLJ proxy for variations in the strength of the CLLJ, shows an apparent coupling of the  $\Delta\text{SST}$  with the low, frequent variations recorded in our Ti data (Fig. 6). Decreases in  $\Delta\text{SST}$  indicate that the Caribbean SST was lower than the value in the Pacific. This could have promoted an increase in the intensity of the CLLJ, since a cold Caribbean Sea favors expansion of the North Atlantic Subtropical High, displacing the CLLJ to the west and thereby increasing humidity in Petén Itzá (Wang, 2007; Lachniet et al., 2009; Fig. 7). During early MIS 3,  $\Delta\text{SST}$  decreased, and it became drier until  $\sim 45$  cal ka BP. After that,  $\Delta\text{SST}$  increased, and wetter conditions occurred around the lake. Although the strength of the CLLJ does not depend solely on the  $\Delta\text{SST}$  between the eastern Pacific and the

Caribbean, but also on the regional topography, the position of the ITCZ and the expansion/contraction of the North Atlantic Subtropical High (NASH; Wang, 2007), we find clear evidence for a close relationship between  $\Delta\text{SST}$  and Ti and hence runoff to Lake Petén Itzá regarding low, frequent variations. This implies that in addition to changes in the ITCZ, spatiotemporal changes are linked to variations in CLLJ that steered the influx of moisture into Petén during MISs 3–2. Additionally the onset of MIS 3, a relatively warm period (Bradley and Diaz, 2021), might have been characterized by a strong NAM, which could have promoted moisture transport from the Caribbean towards northern Mexico. This was shown in records from northern Mexico (e.g., lakes Babicora and Sayulita), where wet interstadials were inferred (Metcalfe et al., 2013; Roy et al., 2013).

### 5.1.2 Mid-MIS 3 (52.7–39.3 cal ka BP): shift to higher evaporation and lower lake levels

The mid-section of MIS 3 corresponds to Unit 5. High Ti (mean  $-0.1 \pm 0.3$ ) and stable quartz contents (mean  $3.2 \pm 2.0\%$ ) indicate that precipitation and runoff to Lake Petén Itzá remained high during the deposition of Unit 5 but were lower than in Unit 6 (Fig. 3). An increase in TOC content (mean  $2.8 \pm 1.0\%$ ) at 51 cal ka BP indicates increased productivity, and a pronounced increase in TOC/TN ratios (mean  $18.7 \pm 5.9$ ) indicates a relatively greater delivery of terrestrial organic matter to the lake (Meyers, 2003). The TOC content reaches maxima in two intervals, around 46.2 and 40.2 cal ka BP, coinciding with increased evaporation (Ca/(Ti + Fe) ratios of up to 5.9). These two periods correlate with peaks in oxic conditions, as suggested by maxima of the Mn/Fe ratio (0.2 and  $-1.6$ ; Fig. 3). Our data thus suggest more oxygenated bottom waters, possibly associated with lower lake levels, which resulted in greater wind-induced mixing of the water column (Yu et al., 1984; Gale et al., 2006). A short-lived increase in runoff terminates Unit 5, a result of more humid conditions that may have delivered greater nutrient loads to the lake. The latter would have favored the input of aquatic organic matter to the sediments between 40.4 and 39.3 cal ka BP. Wetter conditions and greater autochthonous production are supported by high Ti (up to 0.7) and low TOC/TN ratios (6.7), respectively.

A decrease in runoff and lake level lowering, which interrupted the general wet climate during mid-MIS 3, were also inferred by Pérez et al. (2021) from Site PI-6 based on ostracod assemblages that reflect higher conductivity. This was explained by an increase in ion concentrations in the water column associated with higher evaporation / precipitation ratios. In addition, the presence of the high-conductivity-preferring diatom *Cyclotella petenensis* was reported from Site PI-6 sediments between 40 and 39 cal ka BP (Paillès et al., 2018), suggesting high evaporation rates. Enhanced evaporation was associated with an increased contribution of terrestrial organic matter. This may at first appear contradictory.

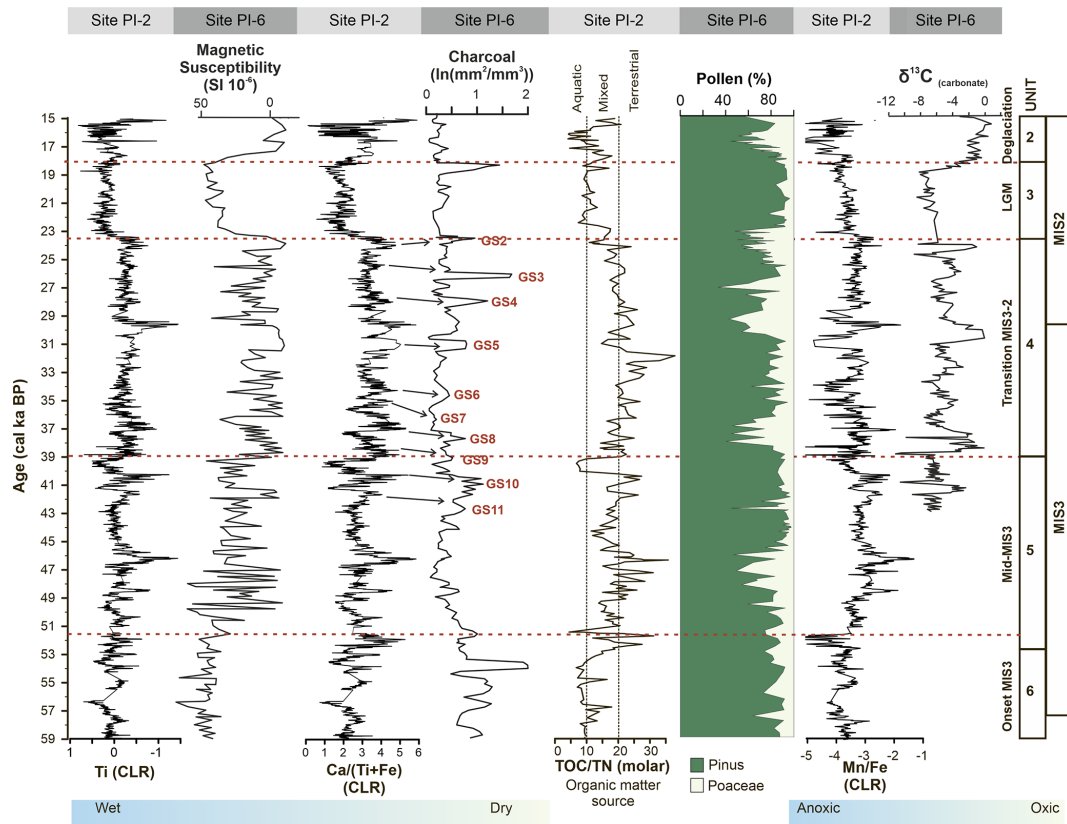


**Figure 4.** Sediment variables in cores from Sites PI-2 and PI-6 (3 km to the west; Fig. 1). Centered log ratio (CLR) values of Ti, Ca/(Ti + Fe) and Mn/Fe. TOC/TN and magnetic susceptibility (Hodell et al., 2008). *Pinus*/*Poaceae* pollen and charcoal datasets (Correa-Metrio et al., 2012) as well as  $\delta^{13}\text{C}$  values from ostracod valves (Escobar et al., 2012). Dashed brown lines indicate unit boundaries described by Mueller et al. (2010).

However, it is consistent with pollen-based support from Site PI-6 for an increase in relative abundance of non-arboreal taxa, e.g., *Poaceae* (grasses) during Unit 5 (Fig. 4; Correa-Metrio et al., 2012). We interpret the increase in terrestrial organic matter as not reflecting changes in the terrestrial vegetation, but rather a shift in the proximity of the plant community (grasslands) to Sites PI-2 and PI-6 because of shrinkage in the lake surface area. This was observed at Lake Tzibaná (southern Mexico) as a consequence of a 20 m decline in water level, during which vegetation colonized subaerially exposed lake bottom, and large amounts of organic matter entered the remnant basin during sporadic periods of rain (Martínez-Abarca et al., 2023).

Whereas our Lake Petén Itzá record – together with other lake and speleothem archives from the circum-Caribbean and Gulf of Mexico, such as Lake Tulane, Florida (Grimm et al., 2006); Abaco Islands, Bahamas (Arienzo et al., 2017); Santo Tomas Cave, Cuba (Warken et al., 2019); and Larga Cave, Puerto Rico (Warken et al., 2020a) – reveals moderately wet conditions during the midst of MIS 3, several paleoclimate records from northern and central Mexico, including those from Lakes Babicora (Roy et al., 2013), Tecoco-

mulco (Caballero et al., 1999), Pátzcuaro (Bradbury, 2000) and Chalco (Ortega-Guerrero et al., 2020), indicate reduced rainfall (Fig. 5). This spatial climate contrast may have been associated with the beginning of the southward migration of the ITCZ. The  $\Delta\text{SST}$  between the eastern Pacific and the Caribbean shows a slight decrease, suggesting that the CLLJ decreased in intensity (Fig. 6), thereby promoting low runoff into Lake Petén Itzá. Nevertheless, climate at Petén Itzá remained relatively humid, possibly attributed to moisture supply associated with a stronger AMOC. Indeed, it has been shown that strengthening of the AMOC may promote enhanced northward heat transport, lower cross-equatorial  $\Delta\text{SST}$  and consequently wetter conditions in the tropical Northern Hemisphere (Fig. 7; Clark et al., 2001; Waelbroeck et al., 2018).

### 5.1.3 MIS 3–2 transition (39.3–23.5 cal ka BP): great hydrological instability

The final stage of MIS 3 and the beginning of MIS 2 correspond to Unit 4. This unit is characterized by high variability in runoff and evaporation. The decrease in Ti (mean  $-0.3 \pm 0.3$ ) indicates a decline in runoff. Moreover, variable

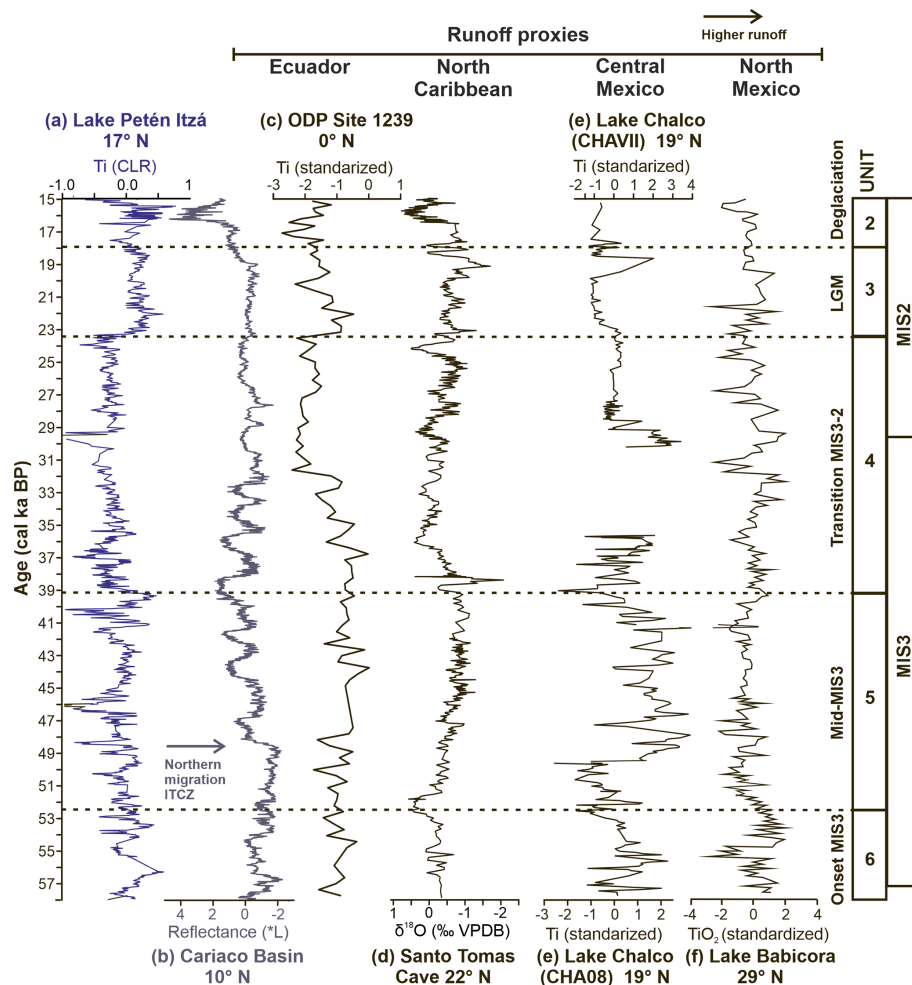


**Figure 5.** Comparison of paleoclimate and runoff/precipitation records spanning MISs 3–2. **(a)** Centered-log-ratio Ti record from Lake Petén Itzá (this study). **(b)** Reflectance data from core MD03-2621, Cariaco Basin (Deplazes et al., 2013b). **(c)** Standardized record of Ti obtained from ODP Site 1239 in the equatorial Pacific Ocean (Rincón-Martínez et al., 2010). **(d)**  $\delta^{18}\text{O}$  data from a stalagmite from Santo Tomas Cave, Cuba (Warren et al., 2019). **(e)** Standardized record of Ti in two sediment sequences from Lake Chalco, central Mexico (Site CHAVII obtained from Lozano-García et al., 2015; CHA08 site obtained from Martínez-Abarca et al., 2021b). **(f)** Standardized  $\text{TiO}_2$  data obtained from Lake Babicora, northern Mexico (Roy et al., 2013). Original data were standardized by subtracting the mean of the data and dividing by the standard deviation.

but higher  $\text{Ca}/(\text{Ti}+\text{Fe})$  ratios (mean  $3.6 \pm 0.7$ ) indicate an increase in evaporation relative to Unit 5 (Fig. 3). In addition, the carbonate content shows a trend similar to that of the Ti dataset. This coupling may suggest an input of detrital carbonate from the karstic bedrock in the catchment. Carbonate in lake sediments is commonly related to (1) inorganic calcite precipitation and consequently to periods of high productivity and/or evaporation and (2) high nutrient input promoting eutrophication, an increase in pH and consequently enhanced biogenic calcite formation (Dean and Megard, 1993; Dean, 1999). Mineralogical data display higher values of gypsum (mean  $53.9 \pm 3.4\%$ ), suggesting drier conditions and hence lower chemical weathering in the catchment. High and stable values of the Mn/Fe ratio (mean  $-3.3 \pm 0.5$ ) indicate oxic bottom waters within this unit, possibly associated with a de-

cline in lake level and greater wind mixing.  $\text{TOC}/\text{TN}$  ratios rapidly increase to values  $> 20$ , suggesting a relative decline in the contribution of aquatic organic matter input relative to that from terrestrial sources. After 32 cal ka BP, however,  $\text{TOC}/\text{TN}$  ratios decreased gradually to values of  $\sim 10$ , indicating a shift once again to dominance of aquatic organic matter. In addition, lower TOC values (mean  $1.9 \pm 1.0\%$ ) in Unit 4 may suggest poor preservation of sediment organic matter as a result of oxidation favored by greater water-column mixing at Site PI-2, as a result of the decline in lake level.

Lower lake levels during the MIS 3–2 transition were inferred previously using the Site PI-6 core (Cohuo et al., 2020; Pérez et al., 2021) from an increase in the relative abundance of the endemic ostracod *Paracythereis opesta*, a

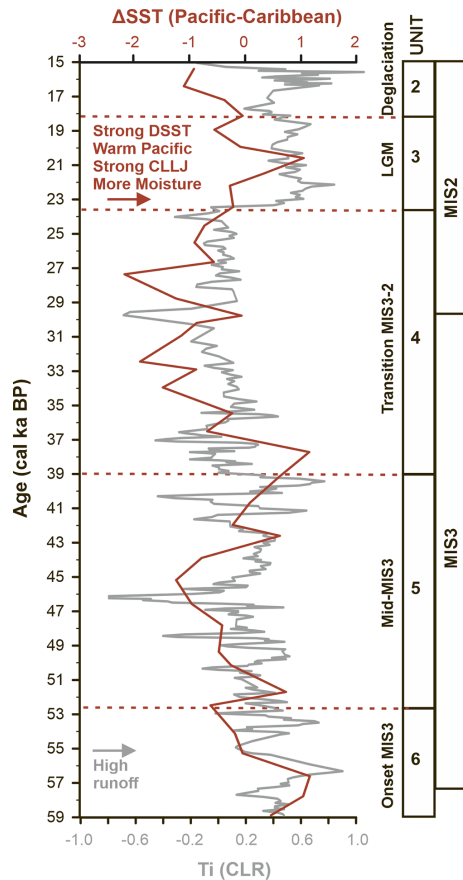


**Figure 6.** Low-frequency co-variability between runoff (Ti) and changes in the intensity of the Caribbean Low-Level Jet (CLLJ). We use the Pacific–Caribbean differences in sea surface temperature ( $\Delta$ SST) as a proxy for the CLLJ. A stronger  $\Delta$ SST, as a consequence of cooling in the Caribbean and/or warming in the Pacific, causes a stronger CLLJ, with more precipitation and runoff at Lake Petén Itzá. Red line:  $\Delta$ SST calculated by subtracting annual SST values inferred from the marine sediment record at Site MD02-2529 in the eastern Pacific (Costa Rica; Leduc et al., 2007b) from values at ODP Site 999A, located in the Caribbean (Schmidt et al., 2006b). Site 999A SST data were obtained using Mg/Ca ratios of the planktonic foraminifera *Globigerinoides ruber*, whereas the MD02-2529 dataset is based on the  $U_{37}^K$ . As the two records possess different temporal resolutions, we approximated the closest ages between both records and subtracted the available SST data. Gray line: Ti from Site PI-2 in Lake Petén Itzá (this study). Ti data were averaged using a LOESS smoothing function (factor=10). The different time periods discussed in the text are linked to the stratigraphic units defined by Mueller et al. (2010).

benthic species associated with shallow-water environments (< 40 m depth) (Cohuo et al., 2017; Echeverría Galindo et al., 2019). In addition, Paillès et al. (2018) found abundant *Cyclotella petenensis* and *C. cassandrae* in deposits from that unit in PI-6. The two diatom species are characteristic of high-conductivity waters, which agrees with our interpretation. Lower water levels, which enabled oxygenation of

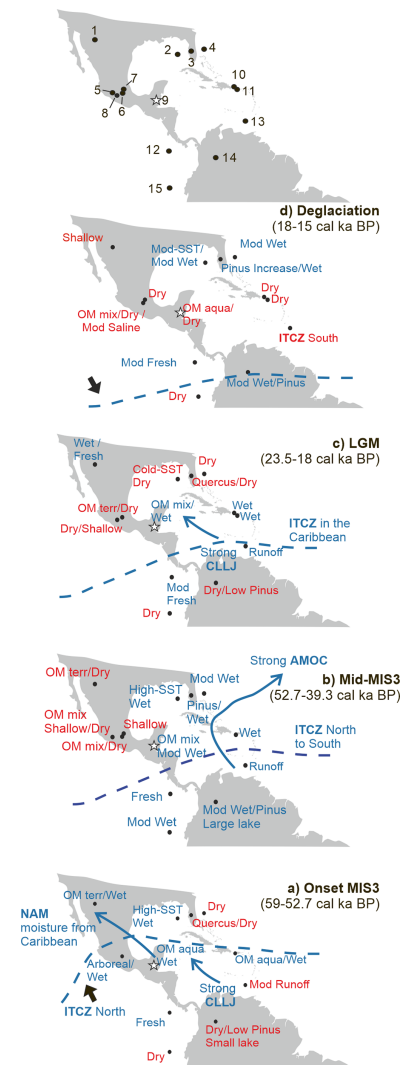


**Figure 7.** Maps showing regional paleoclimate records and limnological/climate characteristics inferred for (a) the onset of MIS 3, (b) mid-MIS 3, (c) the Last Glacial Maximum (LGM) and (d) deglaciation. Blue refers to mainly humid conditions, whereas red indicates primarily dry conditions. Possible mechanisms providing moisture to the northern Neotropics are indicated. Abbreviations: OM aqua (aquatic organic matter), OM terr (terrestrial organic matter), OM mix (mixed organic matter), Mod (moderate), SST (sea surface temperature), AMOC (Atlantic Meridional Overturning Circulation), ITCZ (Intertropical Convergence Zone), CLLJ (Caribbean Low-Level Jet). Records: (1) Lake Babicora (Roy et al., 2013), (2) marine record MD02-2575 (Ziegler et al., 2008), (3) Lake Tulane (Grimm et al., 2006), (4) Bahamian speleothem record AB-DC (Arienzo et al., 2017), (5) Lake Pátzcuaro (Bradbury, 2000), (6) Lake Chalco (Martínez-Abarca et al., 2021b), (7) Lake Tecocomulco (Caballero et al., 1999), (8) Piscina de Yuriria (Holmes et al., 2016), (9) Lake Petén Itzá (this study, marked with a star), (10) Blanchard Cave (Royer et al., 2017), (11) Larga Cave (Warren et al., 2020b), (12) marine record MD02-2529 (Leduc et al., 2007a), (13) Cariaco Basin record MD03-2621 (Deplazes et al., 2013a), (14) Lake Fúquene (Groot et al., 2011), (15) marine record ODP Site 1239 (Rincón-Martínez et al., 2010).

the water column, are also supported by high  $\delta^{13}\text{C}$  values measured in the ostracod *Paracythereis opesta* (previously called *Lymnocythere opesta*) at Site PI-6 (Fig. 4; Escobar et al., 2012). The gradual decrease in runoff, associated with dry conditions inferred from Site PI-2, correlates with a decrease in magnetic susceptibility at Site PI-6 (Fig. 4). On the other hand, the high proportions of terrestrial organic matter prior to 32 cal ka BP coincides with an increase in sediment  $\delta^{13}\text{C}_{\text{TOC}}$  values in the PI-6 record, which was interpreted to reflect a greater proportion of  $\text{C}_4$  plants in the catchment, indicative of drier climate (Mays et al., 2017). The contribution of allochthonous organic matter may also have declined because of the spread of  $\text{C}_4$  savanna vegetation in the lake catchment, with high relative abundances of Cyperaceae and Poaceae (Fig. 4; Correa-Metrio et al., 2012).

Paleoclimate conditions different from those around Lake Petén Itzá were inferred from lakes of central and northern Mexico, where a wetter climate and less saline conditions prevailed (e.g., Lake Babicora, Chávez-Lara et al., 2012; Lake Chalco, Caballero et al., 2019; Fig. 5). This inter-regional comparison of paleoclimate records indicates that the Petén region and northern Gulf of Mexico were dominated by dry conditions during the MIS 3–2 transition. We suggest that during the transition (39.3–23.5 cal ka BP), the ITCZ was mainly located farther south, accounting for the lower precipitation and consequent reduction in runoff to Petén Itzá. The gradual trend towards drier conditions observed after 29 cal ka BP, however, resembles the trend of reduced SST in the eastern Pacific that may have lessened the intensity of the CLLJ, resulting in decreased moisture transport to the Petén region. Therefore, it is possible that much of the runoff to Lake Petén Itzá depended on the position of the CLLJ during the transition.

#### 5.1.4 Last Glacial Maximum (23.5–18.0 cal ka BP): a sudden large increase in runoff

The Last Glacial Maximum (LGM) corresponds to Unit 3, which was studied previously using sediments from Site PI-6 (Hodell et al., 2008; Bush et al., 2009; Pérez et al., 2011; Mays et al., 2017). Ti is highest in Unit 3 and varies between  $-0.6$  and  $1.1$ , reflecting an abrupt increase in humidity and runoff (Fig. 3). This is also supported by the increases in clay and quartz contents (means of  $8.5 \pm 2.9\%$  and  $5.1 \pm 2.5\%$ , respectively).  $\text{Ca}/(\text{Ti}+\text{Fe})$  ratios were lowest in this unit (mean  $1.9 \pm 0.5$ ), indicating substantially reduced rates of evaporation (Fig. 3).  $\text{TOC}/\text{TN}$  ratios  $< 10$  suggest high sedimentation of aquatically derived organic matter. Lower  $\text{Mn}/\text{Fe}$  ratios (mean  $-3.7 \pm 0.3$ ) and generally higher TOC content ( $2.2 \pm 0.6\%$ ) suggest that the deep lake was characterized by persistent bottom-water anoxia that facilitated the preservation of organic matter.

More humid conditions and higher lake levels during the deposition of Unit 3 were also inferred from sediments at Site PI-6. High magnetic susceptibility and density values suggest

high detrital input (Fig. 4; Hodell et al., 2006, 2008), whereas more negative  $\delta^{18}\text{O}$  and  $\delta^{13}\text{C}$  values of ostracod shells indicate higher lake levels and establishment of an anoxic hypolimnion at Site PI-6 (Escobar et al., 2012; Pérez et al., 2013). Ostracod assemblage analysis revealed the presence of deep-water species ( $> 40\text{ m}$  depth) such as *Cypria petenensis* (Pérez et al., 2021), while the presence of the diatom *Discotella gabinii* indicates low-conductivity and alkaline water during the LGM (Paillès et al., 2018).

Wet conditions during the LGM were also inferred from  $\delta^{18}\text{O}$  values in speleothems from the Caribbean region – including those from Blanchard Cave, Guadeloupe (Royer et al., 2017); Larga Cave, Puerto Rico (Warken et al., 2020a); and Santo Tomas Cave, Cuba (Warken et al., 2019) – as well as southwestern (Juxtlahuaca Cave, Guerrero: Lachniet et al., 2014) and northwestern Mexico (Lake Babicora: Metcalfe et al., 2002). In contrast, dry conditions were inferred from other paleoclimate records from central Mexico (e.g., La Piscina de Yuriria: Holmes et al., 2016; Lake Chalco: Lozano-García et al., 2015), the northern Gulf of Mexico (e.g., Lake Tulane, Florida: Grimm et al., 2006; Donders et al., 2011), the Colombia Basin (Lake Fúquene: Groot et al., 2011, 2013; Vriend et al., 2012) and the eastern equatorial Pacific ODP-1239 record (Rincón-Martínez et al., 2010) (Fig. 5). This is consistent with the multi-record analyses of Ramírez-Barahona and Eguiarte (2013), which showed dry conditions for western central Mexico and concomitantly wet conditions in eastern and southern Mexico. Our regional comparison using records from Mexico, the Gulf of Mexico and the Caribbean indicates that the ITCZ may have been positioned mainly over Central America during the LGM (Fig. 7). It is also possible that the decrease in atmospheric temperatures reduced the amount of humidity that entered Mexico from the Caribbean (Hu and Dominguez, 2015). Previous studies showed that during the LGM, an analog to the negative phase of the El Niño Southern–Oscillation (ENSO) persisted, which resulted in a weakening of the NAM, explaining the droughts in central and northern Mexico (Lachniet et al., 2013). The  $\Delta\text{SST}$  suggests that water temperatures in the eastern Pacific were  $\sim 1^\circ\text{C}$  higher than those in the Caribbean during the LGM (Fig. 6), which may have promoted a more intense CLLJ and thus increased moisture transport to the Caribbean, including to the Petén region. This is consistent with estimates from fossil records (e.g., Trend-Staid and Prell, 2002; Kucera et al., 2005) and numerical simulations (e.g., Kitoh and Murakami, 2002; Otto-Bliesner et al., 2009).

#### 5.1.5 Deglaciation (18.0–15.0 cal ka BP): low runoff and enhanced evaporation

At the onset of Unit 2 (18.0–16.3 cal ka BP), a decrease in Ti to 0.1 and an increase in  $\text{Ca}/(\text{Ti}+\text{Fe})$  ratios and gypsum content (averages of  $3.3 \pm 1.4\%$  and  $78.2 \pm 32.8\%$ , respectively) indicate reduced runoff, drier conditions and an in-

crease in evaporation, which would have resulted in lower lake level (Fig. 3). As in Unit 4, carbonate and Ti values are coupled, indicating that input of carbonates into the lake may depend partly on runoff and subsequent precipitation. This is consistent with ostracod-based inferences from Site PI-6 that indicate lower water levels and greater conductivity, with a dominance of littoral ostracod species such as *Cypridopsis vidua*, *Heterocypris putei* and *Paracythereis opesta* (Díaz et al., 2017; Cohuo et al., 2018; Pérez et al., 2021). Likewise, high  $\delta^{18}\text{O}$  values in ostracod shells and gypsum hydration water indicate high evaporation (Escobar et al., 2012; Hodell et al., 2012; Grauel et al., 2016). An estimated 56 m lake level decline was reported by Anselmetti et al. (2006) and Hodell et al. (2006), based on the occurrence of a paleo-shoreline in seismic profiles. Comparatively low TOC/TN ratios at Site PI-2 (mean  $11.5 \pm 4.8$ ) indicate a decrease in the relative contribution of organic matter from terrestrial sources. Furthermore, *n*-alkane distributions in the PI-6 record show reduced loading of terrestrial plant material between 18 and 16 cal ka BP (Mays et al., 2017). This may be explained by the predominance of grassland in the vicinity of the lake (Fig. 4; Bush et al., 2009), which may have contributed little to the sedimentary organic matter.

Dry climate conditions, similar to those at Petén Itzá, were also inferred from sediments in lakes of central Mexico and the Caribbean (Bradbury, 2000; Lozano-García et al., 2015; Royer et al., 2017; Caballero et al., 2019; Martínez-Abarca et al., 2019; Warken et al., 2020a), whereas records from the northern Gulf of Mexico suggest wet conditions that originated from extra-tropical fronts that moved south during the early phase of deglaciation (Ziegler et al., 2008; Donders et al., 2011; Roy et al., 2013; Arienzo et al., 2017). This can be explained by the latitudinal migration of the ITCZ to the south after the LGM and the collapse of the AMOC during HS 1, which promoted dry environments throughout central Mexico and the Caribbean (Fig. 7).

Unit 2 terminates with a sudden increase in Ti (up to 0.8) between 16.3 and 15.0 cal ka BP, indicating an increase in precipitation and runoff. A decrease in Ca/(Ti+Fe) (up to  $-0.1$ ) suggests evaporation remained low, and low TOC/TN ratios ( $< 10.9$ ) indicate a predominance of aquatic organic matter. Although dry conditions may have prevailed at the beginning of the deglaciation corresponding to the first stage of HS 1, the second part (17–15 cal ka BP) was characterized by an increase in runoff and precipitation (Hodell et al., 2012; Pérez et al., 2013). This may have been linked to a slight AMOC recovery that preceded the second stage of HS 1, indicated by lower  $\delta^{18}\text{O}$  values in foraminifera tests from the North Atlantic (McManus et al., 2004).

## 5.2 Millennial-scale climate variability

Whereas long-term transient climate changes have been inferred from multiple records in the region, our high-resolution geochemical records from Site PI-2 also reveal

short-term variations, including abrupt shifts in hydrological proxies between 59 and 15 cal ka BP, similar to those observed in the GICC05 ice-core record from Greenland (Svensson et al., 2008). Low Ca/(Ti+Fe) ratios are associated with high Ti during GIs. This suggests wet conditions and enhanced runoff. Maxima of Ca/(Ti+Fe) and increased gypsum content at Site PI-2 are largely contemporaneous with increases in the  $L^*$  reflectance values in marine core MD03-2621 from the Cariaco Basin, offshore Venezuela (Fig. 8), particularly during GSs 11–2 (Peterson et al., 2000; Deplazes et al., 2013a). Transport of moisture to the Petén region between 42 and 24 cal ka BP seems to have been dominated by changes in SSTs between the eastern Pacific and the Caribbean and in turn by the intensity of the CLLJ. However, variability in runoff and evaporation, suggested by our Ca/(Ti+Fe) ratios during GSs 11–2 and in the Cariaco  $L^*$  reflectance record, may have been largely influenced by millennial-scale changes in the position of the ITCZ.

Maxima in Ca/(Ti+Fe) and hence more humid conditions are more frequent during GSs 11–2. Consequently, the intensity of evaporation (dry conditions) was more pronounced between 42 and 32 cal ka BP, suggesting that the Lake Petén Itzá basin was more susceptible to changes in precipitation, evaporation and drainage during the middle and end of MIS 3. No apparent increases in Ca/(Ti+Fe) were observed during GSs 14–12. However, the Petén Itzá chronology has a  $\pm 2$  kyr uncertainty for ages  $> 45$  cal ka BP, and we therefore cannot exclude the possibility that the Ca/(Ti+Fe) increases at 48.4, 46.2 and 43.8 cal ka BP correspond to low values of  $L^*$  reflectance in the Cariaco Basin record at 49.3 (GS 14), 48.1 (GS 13) and 43.7 (GS 12) cal ka BP, respectively.

The high resolution of the geochemical data, together with the high sedimentation rates at Site PI-2 compared to PI-6, enabled us to study the impact of several GSs on the northern Neotropics (Fig. 8). GSs 11 and 10 show a gradual increase in evaporation over  $\sim 1200$  years, followed by a rapid decrease over  $\sim 400$  years. In contrast, GSs 9–6 started with a rapid increase in evaporation over  $\sim 500$  years that was followed by a gradual reduction in evaporation over  $\sim 1200$  years. This difference is likely explained by changes in the intensity of the CLLJ. During GSs 11 and 10, the CLLJ was stronger and provided more moisture to the region (Fig. 6). Consequently, millennial-scale oscillations in the position of the ITCZ and particularly its displacement to the south were possibly muted by the CLLJ. With respect to GSs 9–6, the intensity of the CLLJ and its capacity to transport moisture decreased, so any millennial-scale change in the ITCZ produced abrupt changes in lake evaporation and catchment runoff. Ca/(Ti+Fe) maxima associated with GSs 5–3 are less pronounced, which may have been a consequence of a weaker CLLJ during the onset of MIS 2, as high values of  $\Delta\text{SST}$  between the Caribbean and eastern Pacific reveal between 34 and 24 cal ka BP. Evidence of GS 2 is missing and may be linked to the onset of the LGM, which was charac-

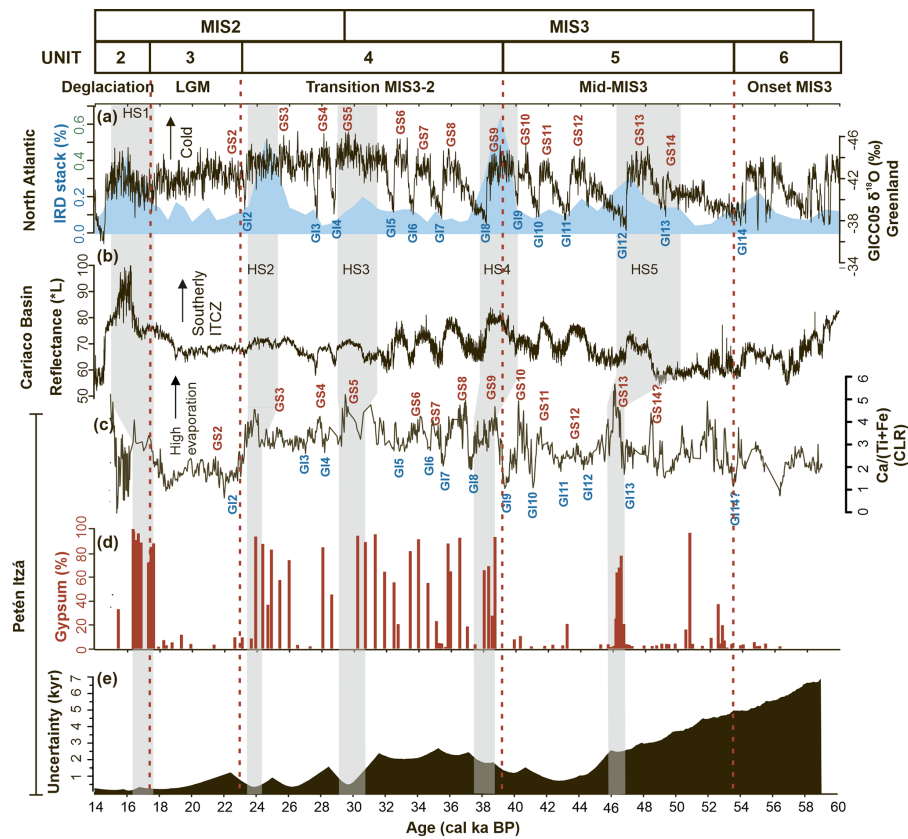


**Figure 8.** Temporal variation in climate proxies in the Petén Itzá PI-2 sediment record compared to other paleoclimate records covering the time span from 60 to 14 cal ka BP. **(a)** North Atlantic ice-rafted debris (IRD) stack derived from 15 individual sediment cores (Lisiecki and Stern, 2016). Oxygen isotopes ( $\delta^{18}\text{O}$ ) from the GICC05 ice core from Greenland (Svensson et al., 2008). More negative values represent colder intervals used to define Greenland stadials (GSs); more positive values represent warmer periods corresponding to Greenland interstadials (GIs). **(b)** Reflectance  $L^*$  from Cariaco Basin sediments, reported by Deplazes et al. (2013b). Higher values indicate a southward migration of the Intertropical Convergence Zone (ITCZ). **(c)** Ca/(Ti+Fe) ratios, **(d)** gypsum content, **(e)** uncertainty in the age–depth model. Gray shaded areas represent HSs.

terized by high humidity in Petén (see Sect. 5.1.4) and may have suppressed the GS 2 signal in the sediment record.

The response to GIs and GSs in Lake Petén Itzá has been studied in sediments from Site PI-6. For example, Correa-Metrio et al. (2012) provided a high-resolution record of pollen and carbonized material ( $\sim 200$ -year resolution), which revealed an increase in forest fires in this region during GSs. This is consistent with high evaporation in response to dry conditions in the northern Neotropics. The latter is more apparent for GS 13, GS 9 and GS 5, whose presence in our record is synchronous with the North Atlantic IRD deposits associated with HSs 5–3, respectively. The enhanced Ca/(Ti + Fe) ratios during GS 13, GS 9 and GS 5 in Lake Petén Itzá may have been a response to dry conditions that dominated during HSs. In addition, higher abundances of gypsum were found during GS 13 and GS 9, suggesting high evaporation of lake water (Fig. 8). Similar increases in Ca/(Ti + Fe) and gypsum content are observed during GS 8, GS 7, GS 5, GS 4 and GS 3. We did not notice an increase in

gypsum content during GS 11, GS 10 and GS 6, which may be related to the low sampling resolution in this interval. The higher Ca/(Ti + Fe) ratios, however, point to an increase in evaporation.

The new age–depth model established here shows that gypsum sand layers were deposited during cold stages HSs 4–1, in agreement with the results of Hodell et al. (2008), Mueller et al. (2010) and Escobar et al. (2012) and with the HS chronology from multiple glacio-marine records across the North Atlantic (Labeyrie et al., 1995; Jullien et al., 2006, 2007; Hodell et al., 2010; Appendix D). With regard to the age uncertainty, HS 5 is likely found between GIs 13 and 12 (49.3–46.0 cal ka BP), also corresponding to a period characterized by gypsum deposition. Lake Petén Itzá sediments associated with HSs 5–1 show Ti below average for the entire sequence, revealing high evaporation and low runoff, associated with dry conditions during their deposition.

Similarities between records from Sites PI-6 and PI-2 confirm the overall suitability of Lake Petén Itzá sediments as a hydroclimate archive. Ostracod data, for example, suggest that HSs 3–1 were characterized by high lake-water conductivity, associated with an increase in evaporation and a reduction in runoff (Cohuo et al., 2018; Pérez et al., 2021). In addition, pollen records show the establishment of savanna vegetation, associated with dry conditions and a drop in MAAT of as much as 6 °C (Correa-Metrio et al., 2012; Hodell et al., 2012). Moreover,  $\delta^{13}\text{C}$  and  $\delta^{18}\text{O}$  values in ostracods indicate a lake level lowering such that Site PI-6 was in such shallow water that the overlying water column did not stratify thermally (Escobar et al., 2012). This is in agreement with paleoclimate records from the eastern equatorial Pacific, the Caribbean and central Mexico (Leduc et al., 2007a; Arienzo et al., 2015, 2017; Medina-Elizalde et al., 2017; Hodell et al., 2017; Caballero et al., 2019), which suggests that HSs 4–1 were generally dry and cold. The drying response of Lake Petén Itzá during HSs correlates with the globally recognized “tropical hydroclimatic events” (THEs), during which extreme regional anomalies in rainfall occurred (Bradley and Diaz, 2021). The dominance of dry conditions in the Caribbean region during THEs was favored by melt-water input to the North Atlantic that, in turn, reduced the AMOC. As a result, the mean position of the ITCZ moved approximately 1° to the south, promoting droughts not only in the northern Neotropics but also in Africa and the Arabian Peninsula (Tjallingii et al., 2008; Zariess et al., 2011).

A key finding of our high-resolution record is confirmation of the abruptness of millennial-scale hydroclimate shifts, which enabled us to link them to AMOC shifts, rather than to gradual longer-term changes caused by orbital forcing, which underlie the short-term, abrupt climate excursions. The spatiotemporal paleoclimate changes (Fig. 7) identified from multiple records across the Neotropics imply that the causes of transient vs. rapid shifts in the region are more complex than mere latitudinal shifts in the ITCZ in response to AMOC. In particular, meridional inter-basin changes in the SST gradient between the Pacific and Atlantic appear to have influenced shifts in the strength and location of deep convection linked to the CLLJ, which steered moisture into some parts of the Neotropics while, other areas were dry. Our results are conceptually consistent with findings from recent climate modeling of the SE Asian monsoon region during the late glacial, which show that regional changes in atmospheric deep convection in response to SST changes can cause strong regional hydroclimate contrasts linked to meridional shifts in low-pressure centers, rather than only latitudinal shifts in the position of the ITCZ (Hällberg et al., 2022).

## 6 Conclusions

We used the sediment record from Site PI-2 in Lake Petén Itzá to infer changes in runoff, evaporation intensity, or-

ganic matter provenance and redox conditions during MISs 3–2 (59–15 cal ka BP). The onset and middle of MIS 3 (59–39.2 cal ka BP) was characterized by periods of high precipitation and runoff into Lake Petén Itzá. At that time, lake levels were high, the lake was very productive, and bottom-water anoxia persisted. The MIS 3–2 transition (39–24 cal ka BP) was characterized by a gradual decline in runoff and an increase in evaporation but was accompanied by high climate variability indicative of regional climate instability. This regime shift was accompanied by input of mixed aquatic and terrestrial organic matter and more oxygenated bottom waters, related to lower lake levels near the end of MIS 3. MIS 2 was a dry period with low runoff, except for the LGM, during which wet conditions prevailed. During the LGM, lake sediments received greater inputs of aquatic organic matter, and the lake hypolimnion was persistently anoxic, presumably associated with incomplete water-column circulation.

Both GSs and GIs were detected in the sediment record at Site PI-2. Compared to previous studies, the record from Site PI-2 provides greater temporal resolution and demonstrates that GSs 9, 8, 7 and 6 began with abrupt increases in evaporation and ended with gradual increases in humidity, whereas GSs 11 and 10 showed the reverse pattern. This can be explained by the lack of moisture transported by the CLLJ during GSs 9–6, which made the local climate susceptible to changes in the latitudinal position of the ITCZ. The high resolution of the PI-2 record highlights the abruptness of climate shifts, which are tied to abrupt changes in the strength of AMOC.

Comparison of our climate proxy records with other terrestrial and marine paleoclimate data from the northern Neotropics, the Caribbean, Florida and northern Mexico indicates that variability in precipitation and, in turn, runoff during MISs 3–2 was strongly influenced by latitudinal shifts in position of the ITCZ in response to changes in the strength of AMOC. Changes in the intensity of the CLLJ and the transport of moisture by the NAM to northern Mexico also influenced fluctuations in runoff. Short-term changes in Ti and Ca/(Ti + Fe) indicate that latitudinal ITCZ variations during MISs 3–2 modified runoff on short (millennial) timescales in response to AMOC shifts, whereas the CLLJ, whose strength/weakness depends on the  $\Delta\text{SST}$  between the Pacific and the Caribbean, among other factors such as the extension of the NASH and interaction with the ITCZ, additionally influenced the ingress of moisture into the region on longer timescales. Whereas our study suggests the importance of inter-basin SST differences in defining regional moisture changes via the strength of the CLLJ on longer timescales, in addition to shifts in the ITCZ, more records and additional modeling studies are required to disentangle the importance of inter-hemispheric changes (ITCZ) and inter-basin changes (CLLJ) on different timescales.

Appendix A

**Table A1.** A total of 31 strata were identified as “slumps” during the development of the age model. Their sedimentology suggests they were deposited rapidly (days to weeks), and consequently their thickness was omitted for age–depth modeling. The omitted deposits include carbonaceous turbidites and volcanic tephras.

Core/section	Top section (cm)	Bottom section (cm)	Top depth (master composite depth, mcd)	Bottom depth (mcd)	Type of deposit	Thickness of deposit (cm)
2D-1H-2	29	33	1.87	1.91	Carbonate turbidite	4
2D-1H-2	35	37	1.93	1.95	Carbonate turbidite	2
2D-2H-2	50	53	5.12	5.15	Carbonate turbidite	3
2D-2H-2	137	139	5.96	5.98	Carbonate turbidite	2
2D-2H-2	142	146	6.01	6.04	Carbonate turbidite	4
2D-3H-1	8	10	6.04	6.06	Carbonate turbidite	2
2D-3H-1	135	137	7.26	7.28	Carbonate turbidite	2
2D-3H-2	40	42	7.8	7.82	Carbonate turbidite	2
2D-3H-2	55	60	7.94	7.99	Carbonate turbidite	5
2A-4H-3	56	62	8.82	8.88	Carbonate turbidite	6
2A-5H-2	28	31	11.76	11.79	Carbonate turbidite	3
2A-5H-2	39	42	11.87	11.9	Carbonate turbidite	3
2A-5H-2	66	73	12.14	12.21	Carbonate turbidite	7
2A-5H-2	100	105	12.48	12.53	Carbonate turbidite	5
2A-5H-2	118	122	12.65	12.69	Carbonate turbidite	4
2D-5H-1	89	90	13.09	13.1	Tephra	1
2D-6H-2	66	68	17.68	17.7	Tephra	2
2A-8H-2	42	44	21.4	21.42	Carbonate turbidite	2
2A-8H-2	58	61	21.56	21.59	Carbonate turbidite	3
2A-8H-2	87	89	21.85	21.87	Carbonate turbidite	2
2A-8H-2	109	111	22.07	22.09	Carbonate turbidite	2
2C-2H-2	91	99	48.15	48.23	Carbonate turbidite	8
2A-19E-2	9	10	54.45	54.46	Tephra	1
2C-6H-1	60	108	57.84	58.32	Carbonate turbidite	48
2C-6H-2	6	14	58.81	58.89	Carbonate turbidite	8
2C-6H-2	29	31	59.04	59.06	Carbonate turbidite	2
2C-6H-2	71	73	59.46	59.48	Carbonate turbidite	2
2C-6H-2	84	87	59.59	59.62	Carbonate turbidite	3
2E-4E-2	0	7	61.43	61.5	Rock	7
2C-9H-1	112	114	64.22	64.24	Tephra	2
2C-9H-2	75	79	65.31	65.35	Carbonate turbidite	4



**Figure A1.** Photographs of two cores from the PI-2 record, showing deposits from short-duration events: (a) carbonate turbidite (PET06-2C-6H-1 core) and (b) tephra C5 (Kutterolf et al., 2016) (PET06-2C-9H-1 core).

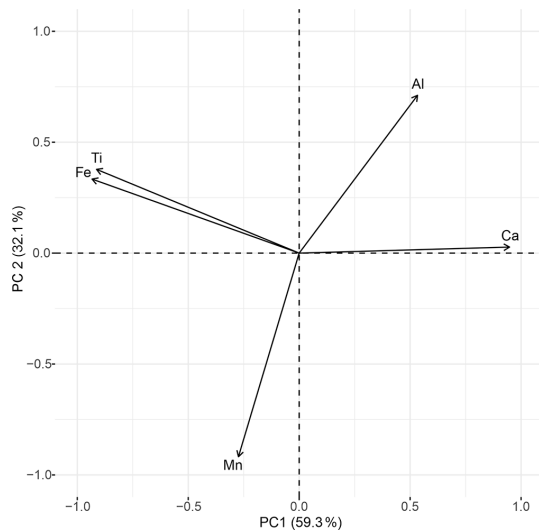


**Figure B1.** Ranking obtained from the PCA for the geochemical variables measured in the PI-2 record. The ordination analysis is related to changes in runoff and evaporation (PC1) and variations in the oxygen content in bottom waters (PC2).

## Appendix B

A principal component analysis (PCA) was carried out to discern the geochemical variables that are related to each other and that potentially respond to the same hydrological variables.

X-ray fluorescence (XRF) data were used. Previously they were weight-averaged with a LOESS smoothing (factor = 3) to remove noise from the signal and were subsequently converted to centered log ratio (CLR). Titanium, aluminum, calcium, iron and manganese were included in the statistical treatment as they are potential indicators of runoff, evaporation and redox processes.

The PCA (Fig. B1) explained more than 91 % of the original variation in the datasets using only the first two principal components. The first principal component (PC1) was mostly associated with detrital elements (Ti, Fe) and those from authigenic mineral formation (Ca) that reflect changes in runoff and evaporation, archived in the sediments. For this reason, we suggest the use of the  $\text{Ca}/(\text{Ti} + \text{Fe})$  ratio as an indicator of evaporation and Ti as a proxy for runoff. PC2 is related to detrital elements (Ti, Fe) and elements related to changing redox conditions at the lake bottom (Mn). As Mn deposition is preferentially favored in oxic environments, we propose the use of  $\text{Mn}/\text{Fe}$  as an indicator of oxic/anoxic conditions at the lake bottom.

## Appendix C

**Table C1.** Main characteristics of Lithological Units 6 to 2 discussed in this study and previously defined by Mueller et al. (2010). We present the depth and age intervals spanned by each unit; the latter values were calculated in this study.

Unit	Depth interval (m)	Age interval (cal ka BP)	Main lithological characteristics
2	24.7–19.0	18.0–15.0	Gypsum-rich deposits composed of massive accumulations of coarse authigenic gypsum crystals and undulating, finely laminated nodular gypsum layers. Clay-rich carbonate consisting of weakly laminated calcite-montmorillonite silt.
3	29.2–24.7	23.5–18.0	Gray submillimeter-scale laminated mud, rich in montmorillonite and calcite. Fragments of reworked gastropods are common.
4	44.0–29.2	39.3–23.5	Gypsum-rich, composed of coarse massive brownish–yellowish gypsum sand and undulating laminated nodular gypsum layers. Clay-rich carbonate, consisting of massive cream-colored silt.
5	60.0–44.0	52.7–39.3	Fine, laminated, clayey mud, rich in organic matter. Up to 5 cm thick graded turbidites are common.
6	67.0–60.0	59–52.7	Gray laminated montmorillonite mud, partly mottled with dark diffuse organic-rich spots, punctuated by one graded dark turbidite sequence of silt. Fragments of reworked gastropods are common.

## Appendix D

**Table D1.** Chronology of Heinrich stadials (HSs) in the PI-2 record compared to glacio-marine records. The <sup>a</sup> refers to the beginning of each HS, and the <sup>b</sup> refers to the time of maximal IRD deposition. MCD: master composite depth.

	Depth Site PI-2 (MCD) (m)	Age Site PI-2 (cal ka BP)	Age (cal ka BP) (Hemming, 2004) <sup>a</sup>	Age (cal ka BP) (Jullien et al., 2006, 2007)	Age (cal ka BP) (Hodell et al., 2010) <sup>b</sup>	Age (cal ka BP) (Lisiecki and Stern, 2016) <sup>b</sup>
HS 1	24.77–22.28	17.7–16.3	16.8	18.3–16.0	16.0	16.0
HS 2	30.13–29.63	24.3–23.7	24.0	26.2–24	24.0	24.5
HS 3	35.37–34.17	31.5–29.4	31.0	31.8–30.2	–	30.5
HS 4	43.99–41.40	39.2–37.5	38.0	40.2–38.2	39.6	39.0
HS 5	51.40–50.80	47.0–46.2	45.0	50.0–47.9	47.5	47.0

**Data availability.** The data can be shared upon request to the author. Eventually, the data will be uploaded to PANGAEA for use by the scientific community.

**Author contributions.** All authors made substantial contributions to the manuscript. RMA, AS, LP and TB directed the research and participated in drafting the manuscript; DH, MB, JC, DA, and FA led the Petén Itzá Scientific Drilling Project. Material used for radiocarbon dating was obtained by TG. MA, PH, DH and SK reviewed the data; MB, DH, SC, LMG, MS, JC, FA, DA, TG, ACM and FS contributed to the interpretation and discussion of the manuscript.

**Competing interests.** The contact author has declared that none of the authors has any competing interests.

**Disclaimer.** Publisher's note: Copernicus Publications remains neutral with regard to jurisdictional claims in published maps and institutional affiliations.

**Acknowledgements.** We thank our many colleagues and the institutions involved in the Petén Itzá Drilling Project. In particular, we thank Andreas Mueller, Jaime Escobar, Adrian Gilli, Florence Sylvestre, Dominik Schmidt, Esmeralda Cruz and Mark Bush as well as Kristina Brady, Anders Noren and others from the National Lacustrine Core Repository (LacCore, now Continental Scientific Drilling – CSD – Facility), University of Minnesota, for their participation and for organizing and providing data. We especially thank Jonathan Obrist-Farner, Rik Tjallingii and Robert Brown for advising and helping during the geochemical analyses and data normalization. We are grateful to Sophie Warken, Sarah Metcalfe, Keely Mills and one anonymous reviewer for comments that improved the manuscript. Funding for this publication was provided by the Deutsche Forschungsgemeinschaft (DFG grants 5448462, 235297191, 252760755, 439719305, KU2685/3-1 and SCHW671/16-1) and Technische Universität Braunschweig. The US National Science Foundation (ATM-0502030), Schweizerischer Nationalfonds zur Förderung der Wissenschaftlichen Forschung (grant 620-066113), Swedish Research Council for Sustainable Development (FORMAS grant 2020-01000) and ICDP provided funding and material support during the drilling campaign.

**Financial support.** This research has been supported by the Deutsche Forschungsgemeinschaft (grant nos. 5448462, 235297191, 252760755, 439719305, KU2685/3-1 and SCHW671/16-1), the US National Science Foundation (grant no. ATM-0502030), the Schweizerischer Nationalfonds zur Förderung der Wissenschaftlichen Forschung (grant no. 620-066113), the Swedish Research Council for Sustainable Development (FORMAS grant 2020-01000) and ICDP.

This open-access publication was funded by Technische Universität Braunschweig.

**Review statement.** This paper was edited by Keely Mills and reviewed by Sarah Metcalfe and one anonymous referee.

## References

- Amador, J. A., Magaña, V. O., and Pérez, J. B.: The low-level jet and convective activity in the Caribbean, in: Proc. 24th Conf. on Hurricanes and Tropical Meteorology American Meteorological Society: Fort Lauderdale, 29 May–2 June 2000, Fort Lauderdale, Florida, 114–115, [https://ams.confex.com/ams/last2000/techprogram/paper\\_12834.htm](https://ams.confex.com/ams/last2000/techprogram/paper_12834.htm) (last access: 17 July 2023), 2000.
- Anselmetti, F. S., Ariztegui, D., Hodell, D. A., Hillesheim, M. B., Brenner, M., Gilli, A., McKenzie, J. A., and Mueller, A. D.: Late Quaternary climate-induced lake level variations in Lake Petén Itzá, Guatemala, inferred from seismic stratigraphic analysis, *Palaeogeogr. Palaeoclimatol. Palaeoecol.*, 230, 52–69, doi:10.1016/j.palaeo.2005.06.037, 2006.
- Arienzo, M. M., Swart, P. K., Pourmand, A., Broad, K., Clement, A. C., Murphy, L. N., Vonhof, H. B., and Kakuk, B.: Bahamas speleothem reveals climate variability associated with Heinrich events. *Earth Planet. Sc. Lett.*, 430, 377–386, <https://doi.org/10.1016/j.epsl.2015.08.035>, 2015.
- Arienzo, M. M., Swart, P. K., Broad, K., Clement, A. C., Pourmand, A., and Kakuk, B.: Multi-proxy evidence of millennial climate variability from multiple Bahamian speleothems, *Quaternary Sci. Rev.*, 161, 18–29, <https://doi.org/10.1016/j.quascirev.2017.02.004>, 2017.
- Bard, E., Rostek, F., Turon, J. L., and Gendreau, S.: Hydrological impact of Heinrich events in the subtropical Northeast Atlantic, *Science*, 289, 1321–1324, <https://doi.org/10.1126/science.289.5483.1321>, 2000.
- Blaauw, M. and Christen, J. A.: Flexible paleoclimate age-depth models using an autoregressive gamma process, *Bayesian Anal.*, 6, 457–474, <https://doi.org/10.1214/11-BA618>, 2011.
- Bloemsma, M. R.: Development of a modelling framework for core data integration using XRF scanning, PhD thesis, Delft University of Technology, Delft, the Netherlands, 229 pp., <https://doi.org/10.4233/uuid:95a90787-edc7-4f1f-9e6a-b2453effabdb>, 2015.
- Boggs, S. (Ed.): Principles of sedimentology and stratigraphy, Pearson Prentice Hall, New Jersey, USA, ISBN 0-13-154728-3, 2006.
- Boyle, J. F.: Organic geochemical methods in palaeolimnology, in: Tracking environmental change using lake sediments, edited by: Last, W. and Smol, J. P., Springer, Dordrecht, the Netherlands, 83–141, ISBN 0-306-47670-3, 2001.
- Bradbury, J. P.: Limnologic history of Lago de Patzcuaro, Michoacan, Mexico for the past 48,000 years: impacts of climate and man, *Palaeogeogr. Palaeoclimatol. Palaeoecol.*, 163, 69–95, [https://doi.org/10.1016/S0031-0182\(00\)00146-2](https://doi.org/10.1016/S0031-0182(00)00146-2), 2000.
- Bradley, R. S. and Diaz, H. F.: Late Quaternary abrupt climate change in the tropics and sub-tropics: The continental signal of Tropical Hydroclimatic Events (THEs), *Rev. Geophys.*, 59, e2020RG000732, <https://doi.org/10.1029/2020RG000732>, 2021.
- Broecker, W., Bond, G., Klas, M., Clark, E., and McManus, J.: Origin of the northern Atlantic's Heinrich events, *Clim. Dynam.*, 6, 265–273, <https://doi.org/10.1007/BF00193540>, 1992.
- Bush, M. B., Correa-Metrio, A. Y., Hodell, D. A., Brenner, M., Anselmetti, F. S., Ariztegui, D., Mueller, A. D., Curtis, J. H., Grzesik, D. A., Burton, C., and Gilli, A.: Re-evaluation of climate change in lowland Central America during the Last Glacial Maximum using new sediment cores from Lake Petén

- Itzá, Guatemala, in: Past climate variability in South America and surrounding regions, edited by: Vimeux, F., Sylvestre, F., and Khodri, M., Springer, Dordrecht, the Netherlands, 113–128, [https://doi.org/10.1007/978-90-481-2672-9\\_5](https://doi.org/10.1007/978-90-481-2672-9_5), 2009.
- Caballero, M., Lozano, S., Ortega, B., Urrutia, J., and Macias, J. L.: Environmental characteristics of Lake Tecocomulco, northern basin of Mexico, for the last 50,000 years, *J. Paleolimnol.*, 22, 399–411, <https://doi.org/10.1023/A:1008012813412>, 1999.
- Caballero, M., Lozano-García, S., Ortega-Guerrero, B., and Correa-Metrio, A.: Quantitative estimates of orbital and millennial scale climatic variability in central Mexico during the last ~40,000 years, *Quaternary Sci. Rev.*, 205, 62–75, <https://doi.org/10.1016/j.quascirev.2018.12.002>, 2019.
- Chávez-Lara, C. M., Roy, P. D., Caballero, M. M., Carreño, A. L., and Lakshumanan, C.: Lacustrine ostracodes from the Chiuhuan Desert of Mexico and inferred Late Quaternary paleoecological conditions, *Rev. Mex. de Cienc. Geol.*, 29, 422–431, 2012.
- Clark, P. U., Marshall, S. J., Clarke, G. K., Hostetler, S. W., Licciardi, J. M., and Teller, J. T.: Freshwater forcing of abrupt climate change during the last glaciation, *Science*, 293, 283–287, <https://doi.org/10.1126/science.1062517>, 2001.
- Cohuo, S., Macario-González, L., Pérez, L., and Schwalb, A.: Overview of Neotropical-Caribbean freshwater ostracode fauna (Crustacea, Ostracoda): identifying areas of endemism and assessing biogeographical affinities, *Hydrobiologia*, 786, 5–21, <https://doi.org/10.1007/s10750-016-2747-1>, 2017.
- Cohuo, S., Macario-González, L., Pérez, L., Sylvestre, F., Pailès, C., Curtis, J. H., Kuterolf, S., Wojewódka, M., Zawisza, E., Szeroczynska, K., and Schwalb, A.: Climate ultrastructure and aquatic community response to Heinrich Stadials (HS5a-HS1) in the continental northern Neotropics, *Quaternary Sci. Rev.*, 197, 75–91, <https://doi.org/10.1016/j.quascirev.2018.07.015>, 2018.
- Cohuo, S., Macario-González, L., Wagner, S., Naumann, K., Echeverría-Galindo, P., Pérez, L., Curtis, J., Brenner, M., and Schwalb, A.: Influence of late Quaternary climate on the biogeography of Neotropical aquatic species as reflected by non-marine ostracodes, *Biogeosciences*, 17, 145–161, <https://doi.org/10.5194/bg-17-145-2020>, 2020.
- Correa-Metrio, A., Bush, M. B., Cabrera, K. R., Sully, S., Brenner, M., Hodell, D. A., Escobar, J., and Guilderson, T.: Rapid climate change and no-analog vegetation in lowland Central America during the last 86,000 years, *Quaternary Sci. Rev.*, 38, 63–75, <https://doi.org/10.1016/j.quascirev.2012.01.025>, 2012.
- Davies, S., Lamb, H., and Roberts, S.: Micro-XRF Core Scanning in Palaeolimnology: Recent Developments, in: *Micro-XRF Studies of Sediment Cores, Developments in Palaeoenvironmental Research Vol. 17*, edited by: Croudace, I. and Rothwell, R., Springer, Dordrecht, the Netherlands, 189–226, [https://doi.org/10.1007/978-94-017-9849-5\\_7](https://doi.org/10.1007/978-94-017-9849-5_7), 2015.
- Dean, W. E.: The carbon cycle and biogeochemical dynamics in lake sediments, *J. Paleolimnol.*, 21, 375–393, <https://doi.org/10.1023/A:1008066118210>, 1999.
- Dean, W. E. and Megard, R. O.: Environment of deposition of CaCO<sub>3</sub> in Elk lake, Minnesota, in: *Elk Lake, Minnesota: Evidence for rapid climate change in the north-central United States*, edited by: Bradbury, J. P. and Dean, E., US Geological Survey, Colorado, USA, 97–115, ISBN 0-8137-2276-4, 1993.
- Deplazes, G., Lückge, A., Peterson, L. C., Timmermann, A., Hamann, Y., Hughen, K. A., Röhl, U., Laj, C., Cane, M. A., Sigman, D. M., and Haug, G. H.: Links between tropical rainfall and North Atlantic climate during the last glacial period, *Nat. Geosci.*, 6, 213–217, <https://doi.org/10.1038/ngeo1712>, 2013a.
- Deplazes, G., Lückge, A., Peterson, L. C., Timmermann, A., Hamann, Y., Hughen, K. A., Röhl, U., Laj, C., Cane, M. A., Sigman, D. M., and Haug, G. H.: Cariaco Basin and Arabian Sea Sediment Reflectance Data Over the Last 100,000 Years, NOAA National Centers for Environmental Information [data set], <https://doi.org/10.25921/2waz-pz97>, 2013b.
- Díaz, K. A., Pérez, L., Correa-Metrio, A., Franco-Gaviria, J. F., Echeverría, P., Curtis, J., and Brenner, M.: Holocene environmental history of tropical, mid-altitude Lake Ocotlito, México, inferred from ostracodes and non-biological indicators, *Holocene*, 27, 1308–1317, <https://doi.org/10.1177/0959683616687384>, 2017.
- Donders, T. H., de Boer, H. J., Finsinger, W., Grimm, E. C., Dekker, S. C., Reichert, G. J., and Wagner-Cremer, F.: Impact of the Atlantic Warm Pool on precipitation and temperature in Florida during North Atlantic cold spells, *Clim. Dynam.*, 36, 109–118, <https://doi.org/10.1007/s00382-009-0702-9>, 2011.
- Dunlea, A. G., Murray, R. W., Tada, R., Alvarez-Zarikian, C. A., Anderson, C. H., Gilli, A., Giosan, L., Gorgas, T., Hennekam, R., Irino T., Murayama, M., Peterson, L., Reichert, G. J., Seki, A., Zheng, H., and Ziegler, M.: Intercomparison of XRF core scanning results from seven labs and approaches to practical calibration, *Geochem. Geophys. Geosy.*, 21, e2020GC009248, <https://doi.org/10.1029/2020GC009248>, 2020.
- Echeverría Galindo, P. G., Pérez, L., Correa-Metrio, A., Aven-daño, C. E., Moguel, B., Brenner, M., Cohuo, S., Macario, L., Caballero, M., and Schwalb, A.: Tropical freshwater ostracodes as environmental indicators across an altitude gradient in Guatemala and Mexico, *Rev. Biol. Trop.*, 67, 1037–1058, <https://doi.org/10.15517/RBT.V67I4.33278>, 2019.
- Engleman, E. E., Jackson, L. L., and Norton, D. R.: Determination of carbonate carbon in geological materials by coulometric titration, *Chem. Geol.*, 53, 125–128, 1985.
- Engstrom, D. R. and Wright Jr., H. E.: Chemical stratigraphy of lake sediments as a record of environmental change, in: *Lake sediments and environmental history: studies in palaeolimnology and palaeoecology in honour of Winifred Tutin*, edited by: Haworth, E. Y. and Lund, J. W. G., Leicester University Press, Leicester, UK, ISBN 9780718512200, 1984.
- Escobar, J., Hodell, D. A., Brenner, M., Curtis, J. H., Gilli, A., Mueller, A. D., Anselmetti, F. S., Ariztegui D., Grzesik, D. A., Pérez, L., Schwalb A., and Guilderson, T. P.: A ~43-ka record of paleoenvironmental change in the Central American lowlands inferred from stable isotopes of lacustrine ostracods, *Quaternary Sci. Rev.*, 37, 92–104, <https://doi.org/10.1016/j.quascirev.2012.01.020>, 2012.
- Friedrich, J., Janssen, F., Aleynik, D., Bange, H. W., Boltacheva, N., Çagatay, M. N., Dale, A. W., Etiopie, G., Erdem, Z., Geraga, M., Gilli, A., Gomoio, M. T., Hall, P. O. J., Hansson, D., He, Y., Holtappels, M., Kirf, M. K., Kononets, M., Kononov, S., Lichtschlag, A., Livingstone, D. M., Marinaro, G., Mazlumyan, S., Naeher, S., North, R. P., Papatheodorou, G., Pfannkuche, O., Prien, R., Rehder, G., Schubert, C. J., Soltwedel, T., Sommer, S., Stahl, H., Stanev, E. V., Teaca, A., Tengberg, A.,

- Waldmann, C., Wehrli, B., and Wenzhöfer, F.: Investigating hypoxia in aquatic environments: diverse approaches to addressing a complex phenomenon, *Biogeosciences*, 11, 1215–1259, <https://doi.org/10.5194/bg-11-1215-2014>, 2014.
- Gale, E., Pattiaratchi, C., and Ranasinghe, R.: Vertical mixing processes in intermittently closed and open lakes and lagoons, and the dissolved oxygen response, *Estuar. Coast. Shelf Sci.*, 69, 205–216, <https://doi.org/10.1016/j.ecss.2006.04.013>, 2006.
- Gibson, K. A. and Peterson, L. C.: A 0.6 million year record of millennial-scale climate variability in the tropics, *Geophys. Res. Lett.*, 41, 969–975, <https://doi.org/10.1002/2013GL058846>, 2014.
- Grauel, A.-L., Hodell, D. A., and Bernasconi, S. M.: Quantitative estimates of tropical temperature change in lowland Central America during the last 42 ka, *Earth Planet. Sc. Lett.*, 438, 37–46, <https://doi.org/10.1016/j.epsl.2016.01.001>, 2016.
- Grimm, E. C., Watts, W. A., Jacobson Jr., G. L., Hansen, B. C., Almquist, H. R., and Dieffenbacher-Krall, A. C.: Evidence for warm wet Heinrich events in Florida, *Quaternary Sci. Rev.*, 25, 2197–2211, <https://doi.org/10.1016/j.quascirev.2006.04.008>, 2006.
- Groot, M. H., Hooghiemstra, H., Berrio, J. C., and Giraldo, C.: North Andean environmental and climatic change at orbital to submillennial time-scales: vegetation, water levels and sedimentary regimes from Lake Fúquene 130–27 ka, *Rev. Palaeobot. Palynol.*, 197, 186–204, <https://doi.org/10.1016/j.revpalbo.2013.04.005>, 2013.
- Groot, M. H. M., Bogotá, R. G., Lourens, L. J., Hooghiemstra, H., Vriend, M., Berrio, J. C., Tuenter, E., Van der Plicht, J., Van Geel, B., Ziegler, M., Weber, S. L., Betancourt, A., Contreras, L., Gaviria, S., Giraldo, C., González, N., Jansen, J. H. F., Konert, M., Ortega, D., Rangel, O., Sarmiento, G., Vandenberghe, J., Van der Hammen, T., Van der Linden, M., and Westerhoff, W.: Ultra-high resolution pollen record from the northern Andes reveals rapid shifts in montane climates within the last two glacial cycles, *Clim. Past*, 7, 299–316, <https://doi.org/10.5194/cp-7-299-2011>, 2011.
- Grousset, F. E., Pujol, C., Labeyrie, L., Auffret, G., and Boelaert, A.: Were the North Atlantic Heinrich events triggered by the behavior of the European ice sheets?, *Geol. J.*, 28, 123–126, [https://doi.org/10.1130/0091-7613\(2000\)28<123:WTNAHE>2.0.CO;2](https://doi.org/10.1130/0091-7613(2000)28<123:WTNAHE>2.0.CO;2), 2000.
- Hällberg, P. L., Schenk, F., Yamoah, K. A., Kuang, X., and Smitenberg, R. H.: Seasonal aridity in the Indo-Pacific Warm Pool during the Late Glacial driven by El Niño-like conditions, *Clim. Past*, 18, 1655–1674, <https://doi.org/10.5194/cp-18-1655-2022>, 2022.
- Heinrich, H.: Origin and consequences of cyclic ice rafting in the Northeast Atlantic Ocean during the past 130,000 years, *Quatern. Res.*, 29, 143–152, [https://doi.org/10.1016/0033-5894\(88\)90057-9](https://doi.org/10.1016/0033-5894(88)90057-9), 1988.
- Hemming, S. R.: Heinrich events: Massive late Pleistocene detritus layers of the North Atlantic and their global climate imprint, *Rev. Geophys.*, 42, RG1005, <https://doi.org/10.1029/2003RG000128>, 2004.
- Hodell, D., Anselmetti, F., Brenner, M., and Ariztegui, D.: The Lake Petén Itzá Scientific Drilling Project, *Sci. Drill.*, 3, 25–29, <https://doi.org/10.2204/ioldp.sd.3.02.2006>, 2006.
- Hodell, D. A., Anselmetti, F. S., Ariztegui, D., Brenner, M., Curtis, J. H., Gilli, A., Grzesik, D.A., Guilderson, T. J., Mueller A. D., Bush, M. B., Correa-Metrio, A., Escobar, J., and Kutterolf, S.: An 85-ka record of climate change in lowland Central America, *Quaternary Sci. Rev.*, 27, 1152–1165, <https://doi.org/10.1016/j.quascirev.2008.02.008>, 2008.
- Hodell, D. A., Evans, H. F., Channell, J. E., and Curtis, J. H.: Phase relationships of North Atlantic ice-rafted debris and surface-deep climate proxies during the last glacial period, *Quaternary Sci. Rev.*, 29, 3875–3886, <https://doi.org/10.1016/j.quascirev.2010.09.006>, 2010.
- Hodell, D. A., Turchyn, A. V., Wiseman, C. J., Escobar, J., Curtis, J. H., Brenner, M., Gilli, A., Mueller, A. D., Anselmetti, F., Ariztegui, D., and Brown, E. T.: Late Glacial temperature and precipitation changes in the lowland Neotropics by tandem measurements of  $\delta^{18}\text{O}$  in biogenic carbonate and gypsum hydration water, *Geochim. Cosmochim. Ac.*, 77, 352–368, <https://doi.org/10.1016/j.gca.2011.11.026>, 2012.
- Hodell, D. A., Nicholl, J. A., Bontognali, T. R., Danino, S., Dorador, J., Dowdeswell, J. A., Einsle, J., Kuhlmann H., Martrat, B., Mleneck-Vautraviers, M. J., Rodríguez-Tovar, F. J., and Röhl, U.: Anatomy of Heinrich Layer 1 and its role in the last deglaciation, *Paleoceanography*, 32, 284–303, <https://doi.org/10.1002/2016PA003028>, 2017.
- Holmes, J. A., Metcalfe, S. E., Jones, H. L., and Marshall, J. D.: Climatic variability over the last 30 000 years recorded in La Piscina de Yuriria, a Central Mexican crater lake, *J. Quaternary Sci.*, 31, 310–324, <https://doi.org/10.1002/jqs.2846>, 2016.
- Hu, H. and Dominguez, F.: Evaluation of oceanic and terrestrial sources of moisture for the North American monsoon using numerical models and precipitation stable isotopes, *J. Hydrometeorol.*, 16, 19–35, <https://doi.org/10.1175/JHM-D-14-0073.1>, 2015.
- IGN – Instituto Geográfico Nacional: IGN (1970) Carta Geológica de la Republica de Guatemala, Esc: 1 : 500,000, <http://www.infoiarna.org.gt/wp-content/uploads/2022/02/Mapa-geologico.pdf> (last access: June 2022), 1970.
- INSIVUMEH – Instituto Nacional de Sismología, Vulcanología, Meteorología e Hidrología: INSIVUMEH (2021) Información meteorológica, <https://insivumeh.gob.gt/> (last access: June 2022), 2021.
- Jaeschke, A., Rühlemann, C., Arz, H., Heil, G., and Lohmann, G.: Coupling of millennial-scale changes in sea surface temperature and precipitation off northeastern Brazil with high-latitude climate shifts during the last glacial period, *Paleoceanogr. Paleoclimatol.*, 22, PA4206, <https://doi.org/10.1029/2006PA001391>, 2007.
- Johnsen S. J., Clausen, H. B., Dansgaard, W., Fuhrert, K., Gundestrup, N., Hammer, C. U., Iversen, P., Jouzel J., Stauffer, B., and Steffensen, J. P.: Irregular glacial interstadials recorded in a new Greenland ice core, *Nature*, 359, 311–313, <https://doi.org/10.1038/359311a0>, 1992.
- Jullien, E., Grousset, F. E., Hemming, S. R., Peck, V. L., Hall, I. R., Jeantet, C., and Billy, I.: Contrasting conditions preceding MIS3 and MIS2 Heinrich events, *Global Planet. Change*, 54, 225–238, <https://doi.org/10.1016/j.gloplacha.2006.06.021>, 2006.
- Jullien, E., Grousset, F., Malaizé, B., Duprat, J., Sanchez-Goni, M. F., Eynaud, F., Charlier, K., Schneider, R., Bory, A., Bout, B., and Flores, J. A.: Low-latitude “dusty events” vs. high-

- latitude “icy Heinrich events, *Quatern. Res.*, 68, 379–386, <https://doi.org/10.1016/j.yqres.2007.07.007>, 2007.
- Kitoh, A. and Murakami, S.: Tropical Pacific climate at the mid-Holocene and the Last Glacial Maximum simulated by a coupled ocean-atmosphere general circulation model, *Paleoceanography*, 17, 1047, <https://doi.org/10.1029/2001PA000724>, 2002.
- Kucera, M., Weinelt, M., Kiefer, T., Pflaumann, U., Hayes, A., Weinelt, M., Chen, M., Mix, A. C., Barrows, T. T., Cortijo, E., Duprat, J., Juggins, S., and Waelbroeck, C.: Reconstruction of sea-surface temperatures from assemblages of planktonic foraminifera: multi-technique approach based on geographically constrained calibration data sets and its application to glacial Atlantic and Pacific Oceans, *Quaternary Sci. Rev.*, 24, 951–998, <https://doi.org/10.1016/j.quascirev.2004.07.014>, 2005.
- Kutterolf, S., Schindlbeck, J. C., Anselmetti, F. S., Ariztegui, D., Brenner, M., Curtis, J., Schmid, D., Hodell, D. A., Mueller, A., Pérez, L., Pérez, W., Schwalb, A., Frische, M., and Wang, K. L.: A 400-ka tephrochronological framework for Central America from Lake Petén Itzá (Guatemala) sediments, *Quaternary Sci. Rev.*, 150, 200–220, <https://doi.org/10.1016/j.quascirev.2016.08.023>, 2016.
- Labeyrie, L., Vidal, L., Cortijo, E., Paterne, M., Arnold, M., Duplessy, J. C., Vautravers, M. L., Labracherie, M., Duprat, J., Turon, J. L., Grousset, F. E., and van Weering, T.: Surface and deep hydrology of the northern Atlantic Ocean during the past 150,000 years, *Philos. T. Roy. Soc. Lond.*, 348, 255–264, <https://doi.org/10.1098/rstb.1995.0067>, 1995.
- Lachniet, M. S., Johnson, L., Asmerom, Y., Burns, S. J., Polyak, V., Patterson, W. P., and Azouz, A.: Late Quaternary moisture export across Central America and to Greenland: evidence for tropical rainfall variability from Costa Rican stalagmites, *Quaternary Sci. Rev.*, 28, 3348–3360, <https://doi.org/10.1016/j.quascirev.2009.09.018>, 2009.
- Lachniet, M. S., Asmerom, Y., Bernal, J. P., Polyak, V. J., and Vazquez-Selem, L.: Orbital pacing and ocean circulation-induced collapses of the Mesoamerican monsoon over the past 22,000 yr, *P. Natl. Acad. Sci. USA*, 110, 9255–9260, <https://doi.org/10.1073/pnas.1222804110>, 2013.
- Lachniet, M. S., Denniston, R. F., Asmerom, Y., and Polyak, V. J.: Orbital control of western North America atmospheric circulation and climate over two glacial cycles, *Nat. Commun.*, 5, 1–8, <https://doi.org/10.1038/ncomms4805>, 2014.
- Last, W. M.: Mineralogical analysis of lake sediments, in: *Tracking environmental change using lake sediments*, edited by: Last, W. and Smol, J. P., Springer, Dordrecht, the Netherlands, 143–187, ISBN 0-306-47670-3, 2001.
- Leduc, G., Vidal, L., Tachikawa, K., Rostek, F., Sonzogni, C., Beaufort, L., and Bard, E.: Moisture transport across Central America as a positive feedback on abrupt climatic changes, *Nature*, 445, 908–911, <https://doi.org/10.1038/nature05578>, 2007a.
- Leduc, G., Vidal, L., Tachikawa, K., Rostek, F., Sonzogni, C., Beaufort, L., and Bard, E.: Eastern Equatorial Pacific (MD02-2529) 90 KYr SST and SSS Reconstructions, NOAA National Centers for Environmental Information [data set], <https://doi.org/10.25921/qr9a-na19>, 2007b.
- Lisiecki, L. E. and Raymo, M. E.: A Pliocene-Pleistocene stack of 57 globally distributed benthic  $\delta^{18}\text{O}$  records, *Paleoceanography*, 20, PA1003, <https://doi.org/10.1029/2004PA001071>, 2005.
- Lisiecki, L. E. and Stern, J. V.: Regional and global benthic  $\delta^{18}\text{O}$  stacks for the last glacial cycle, *Paleoceanogr. Paleoclimatol.*, 31, 1368–1394, <https://doi.org/10.1002/2016PA003002>, 2016.
- Löwenberg-Neto, P.: Neotropical region: a shapefile of Morone’s (2014) biogeographical regionalization, *Zootaxa*, 3802, 300–300, <https://doi.org/10.11646/zootaxa.3802.2.12>, 2014.
- Lozano-García, S., Ortega, B., Roy, P. D., Beramendi-Orosco, L., and Caballero, M.: Climatic variability in the northern sector of the American tropics since the latest MIS 3, *Quatern. Res.*, 84, 262–271, <https://doi.org/10.1016/j.yqres.2015.07.002>, 2015.
- Lozano-García, S., Torres-Rodríguez, E., Figueroa-Rangel, B., Caballero, M., Sosa-Nájera, S., Ortega-Guerrero, B., and Acosta-Noriega, C.: Vegetation history of a Mexican Neotropical basin from the late MIS 6 to early MIS 3: The pollen record of Lake Chalco, *Quaternary Sci. Rev.*, 297, 107830, <https://doi.org/10.1016/j.quascirev.2022.107830>, 2022.
- Macario-González, L., Cohuo, S., Hoelzmann, P., Pérez, L., Elías-Gutiérrez, M., Caballero, M., and Schwalb, A.: Geodiversity influences limnological conditions and freshwater ostracode species distributions across broad spatial scales in the northern Neotropics, *Biogeosciences*, 19, 5167–5185, <https://doi.org/10.5194/bg-19-5167-2022>, 2022.
- Martínez-Abarca, R., Lozano-García, S., Ortega-Guerrero, B., and Caballero-Miranda, M.: Incendios y actividad volcánica: historia de fuego en la cuenca de México en el Pleistoceno tardío con base en registros de material carbonizado en el lago de Chalco, *Rev. Mex. de Cienc. Geol.*, 36, 259–269, 2019.
- Martínez-Abarca, L. R., Lozano-García, S., Ortega-Guerrero, B., Chávez-Lara, C. M., Torres-Rodríguez, E., Caballero, M., Brown, E. T., Sosa-Nájera, S., Acosta-Noriega, C., and Sandoval-Ibarra, V.: Environmental changes during MIS6-3 in the Basin of Mexico: A record of fire, lake productivity history and vegetation, *J. S. Am. Earth Sci.*, 109, 103231, <https://doi.org/10.1016/j.jsames.2021.103231>, 2021a.
- Martínez-Abarca, R., Ortega-Guerrero, B., Lozano-García, S., Caballero, M., Valero-Garcés, B., McGee, D., Brown, E. T., Stockhecke, M., and Hodgetts, A. G.: Sedimentary stratigraphy of Lake Chalco (Central Mexico) during its formative stages, *Int. J. Earth Sci.*, 110, 2519–2539, <https://doi.org/10.1007/s00531-020-01964-z>, 2021b.
- Martínez-Abarca, R., Bücker, M., Hoppenbrock, J., Flores-Orozco, A., Pita de la Paz, C., Fröhlich, K., Buckel, J., Lauke, T., Moguel, B., Bonilla, M., Rubio-Sandoval, K., Echeverría-Galindo, P., Landois, S., García, M., Caballero, M., Rodríguez, S., Morales, W., Escolero, O., Correa-Metrio, A., Wojewódka-Przybył, M., Schwarz, A., Krahn, K., Schwalb, A., and Pérez, L.: Evidence of large water-level variations found in deltaic sediments of a tropical deep lake in the karst mountains of the Lacandon forest, Mexico, *J. Paleolimnol.*, 69, 99–121, <https://doi.org/10.1007/s10933-022-00264-7>, 2023.
- Mason, B. and Moore, C. B. (Eds.): *Principles of geochemistry*, in: 4th Edn., John Wiley & Sons, New York, USA, ISBN 3-432-94611-2, 1982.
- Mays, J. L., Brenner, M., Curtis, J. H., Curtis, K. V., Hodell, D. A., Correa-Metrio, A., Escobar, J., Dutton, A. L., Zimmerman, A. R., and Guilderson, T. P.: Stable carbon isotopes ( $\delta^{13}\text{C}$ ) of total organic carbon and long-chain n-alkanes as proxies for climate and environmental change in a sediment core

- from Lake Petén-Itzá, Guatemala, *J. Paleolimnol.*, 57, 307–319, <https://doi.org/10.1007/s10933-017-9949-z>, 2017.
- McManus, J., Francois, R., Gherardi, J. M., Keigwin, L. D., and Brown-Leger, S.: Collapse and rapid resumption of Atlantic meridional circulation linked to deglacial climate changes, *Nature*, 428, 834–837, <https://doi.org/10.1038/nature02494>, 2004.
- Medina-Elizalde, M., Burns, S. J., Polanco-Martinez, J., Lasas-Hernández, F., Bradley, R., Wang, H. C., and Shen, C. C.: Synchronous precipitation reduction in the American Tropics associated with Heinrich 2, *Sci. Rep.*, 7, 1–12, <https://doi.org/10.1038/s41598-017-11742-8>, 2017.
- Metcalf, S., Say, A., Black, S., McCulloch, R., and O’Hara, S.: Wet conditions during the last glaciation in the Chihuahuan Desert, Alta Babicora Basin, Mexico, *Quatern. Res.*, 57, 91–101, <https://doi.org/10.1006/qres.2001.2292>, 2002.
- Metcalf, S. E., Barron, J. A., Roy, P., and Davies, S.: Late Quaternary change in the North American (Mexican) Monsoon: variability in terrestrial and marine records and possible mechanisms, in: AGU Spring Meeting Abstracts, USA, May 2013, May 2013, San Francisco, USA, PP43A-02, <https://ui.adsabs.harvard.edu/abs/2013AGUSMPP43A..02M/abstract> (last access: 17 July 2023), 2013.
- Meyers, P. A.: Applications of organic geochemistry to paleolimnological reconstructions: a summary of examples from the Laurentian Great Lakes, *Org. Geochem.*, 34, 261–289, [https://doi.org/10.1016/S0146-6380\(02\)00168-7](https://doi.org/10.1016/S0146-6380(02)00168-7), 2003.
- Meyers, P. A. and Ishiwatari, R.: Organic matter accumulation records in lake sediments, in: *Physics and chemistry of lakes*, edited by: Lerman, A., Imboden, D. M., and Ga, J. R., Springer, Berlin, Germany, 279–328, [https://doi.org/10.1007/978-3-642-85132-2\\_10](https://doi.org/10.1007/978-3-642-85132-2_10), 1995.
- Moernaut, J., Van Daele, M., Strasser, M., Clare, M. A., Heirman, K., Viel, M., Cardenas, J., Kilian, R., Ladron de Guevara, B., Pino, M., Urrutia, R., and De Batist, M.: Lacustrine turbidites produced by surficial slope sediment remobilization: a mechanism for continuous and sensitive turbidite paleoseismic records, *Mar. Geol.*, 384, 159–176, <https://doi.org/10.1016/j.margeo.2015.10.009>, 2017.
- Mueller, A. D.: Late Quaternary Environmental Change in the Lowland Neotropics: The Petén Itzá Scientific Drilling Project, Guatemala, PhD thesis, ETH Zurich, Zurich, Switzerland, 129 pp., <https://doi.org/10.3929/ethz-a-005927704>, 2009.
- Mueller, A. D., Anselmetti, F. S., Ariztegui, D., Brenner, M., Hodell, D. A., Curtis, J. H., Escobar, J., Guilli, A., Grzesik, D. A., Guilderson, T. P., Kutterolf, S., and Plötze, M.: Late Quaternary palaeoenvironment of northern Guatemala: evidence from deep drill cores and seismic stratigraphy of Lake Petén Itzá, *Sedimentology*, 57, 1220–1245, <https://doi.org/10.1111/j.1365-3091.2009.01144.x>, 2010.
- Mulder, T., Gillet, H., Hanquiez, V., Reijmer, J. J. G., Droxler, A. W., Recouvreur, A. G., Fabregas, N., Cavailles, T., Fauquembergue, K., Blank, D. G., Guiastrenec, L. Seibert, C. Bashah, S., Bujan, S., Ducassou, E., Principaud, M., Conesa, G., Le Goff, J., Ragusa, J., Busson, J., and Borgomano, J.: Into the deep: A coarse-grained carbonate turbidite valley and canyon in ultra-deep carbonate setting, *Mar. Geol.*, 407, 316–333, <https://doi.org/10.1016/j.margeo.2018.11.003>, 2019.
- Naeher, S., Gilli, A., North, R. P., Hamann, Y., and Schubert, C. J.: Tracing bottom water oxygenation with sedimentary Mn/Fe ratios in Lake Zurich, Switzerland, *Chem. Geol.*, 352, 125–133, <https://doi.org/10.1016/j.chemgeo.2013.06.006>, 2013.
- Ortega-Guerrero, B., Avendaño, D., Caballero, M., Lozano-García, S., Brown, E. T., Rodríguez, A., García, B., Barceinas, H., Soler, M. A., and Albarrán, A.: Climatic control on magnetic mineralogy during the late MIS 6–Early MIS 3 in Lake Chalco, central Mexico, *Quaternary Sci. Rev.*, 230, 106163, <https://doi.org/10.1016/j.quascirev.2020.106163>, 2020.
- Otto-Bliesner, B. L., Schneider, R., Brady, E. C., Kucera, M., Abe-Ouchi, A., Bard, E., Braconnot, P., Crucifix, M., Hewitt, C. D., Kageyama, M., Marti, O., Paul, A., Rosell-Melé, A., Waelbroeck, C., Weber, S. L., Weinelt, M., and Yu, Y.: A comparison of PMIP2 model simulations and the MARGO proxy reconstruction for tropical sea surface temperatures at last glacial maximum, *Clim. Dynam.*, 32, 799–815, <https://doi.org/10.1007/s00382-008-0509-0>, 2009.
- Paillès, C., Sylvestre, F., Escobar, J., Tonetto, A., Rustig, S., and Mazur, J. C.: *Cyclotella petenensis* and *Cyclotella cassandrae*, two new fossil diatoms from Pleistocene sediments of Lake Petén-Itzá, Guatemala, Central America, *Phytotaxa*, 351, 247–263, <https://doi.org/10.11646/phytotaxa.351.4.1>, 2018.
- Pérez, L., Frenzel, P., Brenner, M., Escobar, J., Hoelzmann, P., Scharf, B., and Schwalb, A.: Late Quaternary (24–10 ka BP) environmental history of the Neotropical lowlands inferred from ostracodes in sediments of Lago Petén Itzá, Guatemala, *J. Paleolimnol.*, 46, 59–74, <https://doi.org/10.1007/s10933-011-9514-0>, 2011.
- Pérez, L., Curtis, J., Brenner, M., Hodell, D., Escobar, J., Lozano, S., and Schwalb, A.: Stable isotope values ( $\delta^{18}\text{O}$  &  $\delta^{13}\text{C}$ ) of multiple ostracode species in a large Neotropical lake as indicators of past changes in hydrology, *Quaternary Sci. Rev.*, 66, 96–111, <https://doi.org/10.1016/j.quascirev.2012.10.044>, 2013.
- Pérez, L., Correa-Metrio, A., Cohuo, S., González, L. M., Echeverria-Galindo, P., Brenner, M., Curtis, J., Kutterolf, S., Stockhecke, M., Schenk, F., Bauersachs, T., and Schwalb, A.: Ecological turnover in neotropical freshwater and terrestrial communities during episodes of abrupt climate change, *Quatern. Res.*, 101, 26–36, <https://doi.org/10.1017/qua.2020.124>, 2021.
- Peterson, L. C., Haug, G. H., Hughen, K. A., and Röhl, U.: Rapid changes in the hydrologic cycle of the tropical Atlantic during the last glacial, *Science*, 290, 1947–1951, <https://doi.org/10.1126/science.290.5498.1947>, 2000.
- Ramírez-Barahona, S. and Eguiarte, L. E.: The role of glacial cycles in promoting genetic diversity in the Neotropics: the case of cloud forests during the Last Glacial Maximum, *Ecol. Evol.*, 3, 725–738, <https://doi.org/10.1002/ece3.483>, 2013.
- R Core Team: R: a language and environment for statistical computing, R Foundation for Statistical Computing, Vienna, <https://www.R-project.org> (last access: January 2023), 2018.
- Reimer, P. J., Austin, W. E. N., Bard, E., Bayliss, A., Blackwell, P. G., Raymsey, C. B., Butzin, M., Cheng, H., Edwards, R. L., Friedrich, M., Grootes, P. M., Guilderson, T. P., Hajdas, I., Heaton, T. J., Hogg, A. G., Hughen, K. A., Kromer, B., Manning, S. W., Muscheler, R., Palmer, J. G., Pearson, C., Van der Plicht, J., Reimer, R. W., Richards, D. A., Scott, E. M., Saurhohn, J. R., Turney, C. S. M., Wacker, L., Adolphi, F., Büntgen, U., Capano, M., Fahrni, S. M., Fogtmann-Schulz, A., Friedrich, R., Köhler, P., Kudsk, S., Miyake, F., Olsen, J., Reining, F., Sakamoto, M., Sookdeo, A., and Talamo, S.: The IntCal20 Northern Hemisphere

- radiocarbon age calibration curve (0–55 cal BP), *Radiocarbon*, 62, 725–757, <https://doi.org/10.1017/RDC.2020.41>, 2020.
- Rincón-Martínez, D., Lamy, F., Contreras, S., Leduc, G., Bard, E., Saukel, C., Blanz, T., Mackensen, A., and Tiedemann, R.: More humid interglacials in Ecuador during the past 500 kyr linked to latitudinal shifts of the equatorial front and the Intertropical Convergence Zone in the eastern tropical Pacific, *Paleoceanography*, 25, PA2210, <https://doi.org/10.1029/2009PA001868>, 2010.
- Roy, P. D., Quiroz-Jiménez, J. D., Pérez-Cruz, L. L., Lozano-García, S., Metcalfe, S. E., Lozano-Santacruz, R., López-Balbiaux, N., Sánchez-Zavala, J. L., and Romero, F. M.: Late Quaternary paleohydrological conditions in the drylands of northern Mexico: a summer precipitation proxy record of the last 80 cal ka BP, *Quaternary Sci. Rev.*, 78, 342–354, <https://doi.org/10.1016/j.quascirev.2012.11.020>, 2013.
- Royer, A., Malaizé, B., Lécuyer, C., Queffelec, A., Charlier, K., Caley, T., and Lenoble, A.: A high-resolution temporal record of environmental changes in the Eastern Caribbean (Guadeloupe) from 40 to 10 ka BP, *Quaternary Sci. Rev.*, 155, 198–212, <https://doi.org/10.1016/j.quascirev.2016.11.010>, 2017.
- Schmidt, M. W., Vautravers, M. J., and Spero, H. J.: Western Caribbean sea surface temperatures during the late Quaternary, *Geochem. Geophys. Geosyst.*, 7, Q02P10, <https://doi.org/10.1029/2005GC000957>, 2006a.
- Schmidt, M. W., Vautravers, M. J., and Spero, H. J.: Western Caribbean ODP 999A Mg/Ca and  $\delta^{18}\text{O}$  Data and SST Reconstruction, NOAA National Centers for Environmental Information [data set], <https://doi.org/10.25921/xfg0-xk62>, 2006b.
- Simmons, C. S., Tarano, J. M., and Pinto, J. H. (Eds.): Clasificación de reconocimiento de los suelos de la República de Guatemala, Ministerio de Agricultura, Guatemala City, Guatemala, <https://searchworks.stanford.edu/view/5513257> (last access: March 2022), 1959.
- Spence, J. M., Taylor, M. A., and Chen, A. A.: The effect of concurrent seasurface temperature anomalies in the tropical Pacific and Atlantic on Caribbean rainfall, *Int. J. Climatol.*, 24, 1531–1541, <https://doi.org/10.1002/joc.1068>, 2004.
- Svensson, A., Andersen, K. K., Bigler, M., Clausen, H. B., Dahl-Jensen, D., Davies, S. M., Johnsen, S. J., Muscheler, R., Parrenin, F., Rasmussen, S. O., Röthlisberger, R., Seierstad, I., Steffensen, J. P., and Vinther, B. M.: A 60 000 year Greenland stratigraphic ice core chronology, *Clim. Past*, 4, 47–57, <https://doi.org/10.5194/cp-4-47-2008>, 2008.
- Talbot, M. R. and Johannessen, T.: A high resolution palaeoclimatic record for the last 27,500 years in tropical West Africa from the carbon and nitrogen isotopic composition of lacustrine organic matter, *Earth Planet. Sc. Lett.*, 110, 23–37, [https://doi.org/10.1016/0012-821X\(92\)90036-U](https://doi.org/10.1016/0012-821X(92)90036-U), 1992.
- Tjallingii, R., Claussen, M., Stuut, J. B. W., Fohlmeister, J., Jahn, A., Bickert, T., Lamy, F., and Röhl, U.: Coherent high- and low-latitude control of the northwest African hydrological balance, *Nat. Geosci.*, 1, 670–675, <https://doi.org/10.1038/ngeo289>, 2008.
- Trend-Staid, M. and Prell, W. L.: Sea surface temperature at the Last Glacial Maximum: A reconstruction using the modern analog technique, *Paleoceanography*, 17, 1065, <https://doi.org/10.1029/2000PA000506>, 2002.
- Van De Kamp, P. C.: Arkose, subarkose, quartz sand, and associated muds derived from felsic plutonic rocks in glacial to tropical humid climates, *J. Sediment. Res.*, 80, 895–918, <https://doi.org/10.2110/jsr.2010.081>, 2010.
- Vriend, M., Groot, M. H. M., Hooghiemstra, H., Bogotá-Angel, R. G., and Berrio, J. C.: Changing depositional environments in the Colombian Fúquene Basin at submillennial time-scales during 284–27 ka from unmixed grain-size distributions and aquatic pollen, *Neth. J. Geosci.*, 91, 199–214, <https://doi.org/10.1017/S0016774600001591>, 2012.
- Waelbroeck, C., Pichat, S., Böhm, E., Loughheed, B. C., Faranda, D., Vrac, M., Missiaen, L., Vazquez Riveiros, N., Burckel, P., Lippold, J., Arz, H. W., Dokken, T., and Dapigny, A.: Relative timing of precipitation and ocean circulation changes in the western equatorial Atlantic over the last 45 kyr, *Clim. Past*, 14, 1315–1330, <https://doi.org/10.5194/cp-14-1315-2018>, 2018.
- Wang, C.: Variability of the Caribbean low-level jet and its relations to climate, *Clim. Dynam.*, 29, 411–422, <https://doi.org/10.1007/s00382-007-0243-z>, 2007.
- Warren, S. F., Scholz, D., Spötl, C., Jochum, K. P., Pajón, J. M., Bahr, A., and Mangini, A.: Caribbean hydroclimate and vegetation history across the last glacial period, *Quaternary Sci. Rev.*, 218, 75–90, <https://doi.org/10.1016/j.quascirev.2019.06.019>, 2019.
- Warren, S. F., Vieten, R., Winter, A., Spötl, C., Miller, T. E., Jochum, K. P., Schröder-Ritzrau, A., Mangini, A., and Scholz, D.: Persistent link between Caribbean precipitation and Atlantic Ocean circulation during the Last Glacial revealed by a speleothem record from Puerto Rico, *Paleoceanogr. Paleoclimatol.*, 35, e2020PA003944, <https://doi.org/10.1029/2020PA003944>, 2020a.
- Warren, S. F., Scholz, D., Spötl, C., Jochum, K. P., Pajon, J. M., Bahr, A., and Mangini, A.: Stable isotopes covering 96–7 ka BP from stalagmite CM (Santo Tomas Cave, Cuba), PANGAEA [data set], <https://doi.org/10.1594/PANGAEA.912646>, 2020b.
- Weltje, G., Bloemsmas, M., Tjallingii, R., Heslop, D., Röhl, U., and Croudace, I.: Prediction of Geochemical Composition from XRF Core Scanner Data: A New Multivariate Approach Including Automatic Selection of Calibration Samples and Quantification of Uncertainties, in: *Micro-XRF Studies of Sediment Core*, edited by: Croudace, I. and Rothwell, R., Springer, Dordrecht, the Netherlands, [https://doi.org/10.1007/978-94-017-9849-5\\_21](https://doi.org/10.1007/978-94-017-9849-5_21), 2015.
- Weltje, G. J. (Ed.): Provenance and dispersal of sand-sized sediments: Reconstruction of dispersal patterns and sources of sand-sized sediments by means of inverse modelling techniques, Utrecht University, Utrecht, the Netherlands, <https://dspace.library.uu.nl/handle/1874/274730> (last access: May 2022), 1994.
- Wersin, P., Höhener, P., Giovanoli, R., and Stumm, W.: Early diagenetic influences on iron transformations in a freshwater lake sediment, *Chem. Geol.*, 90, 233–252, [https://doi.org/10.1016/0009-2541\(91\)90102-W](https://doi.org/10.1016/0009-2541(91)90102-W), 1991.
- Whyte, F. S., Taylor, M. A., Stephenson, T. S., and Campbell, J. D.: Features of the Caribbean low level jet, *Int. J. Climatol.*, 28, 119–128, <https://doi.org/10.1002/joc.1510>, 2008.
- Yarincik, K. M., Murray, R. W., and Peterson, L. C.: Climatically sensitive eolian and hemipelagic deposition in the Cariaco Basin, Venezuela, over the past 578,000 years: Results from Al/Ti and K/Al, *Paleoceanography*, 15, 210–228, <https://doi.org/10.1029/1999PA900048>, 2000.

- Yu, S. L., Hamrick, J. M., and Lee, D.: Wind Effects on Air-Water Oxygen Transfer in a Lake, in: Gas Transfer at Water Surfaces. Water Science and Technology Library, vol. 2, edited by: Brutsaert, W. and Jirka, G. H., Springer, Dordrecht, the Netherlands, [https://doi.org/10.1007/978-94-017-1660-4\\_33](https://doi.org/10.1007/978-94-017-1660-4_33), 1984.
- Zarriess, M., Johnstone, H., Prange, M., Steph, S., Groeneveld, J., Mulitza, S., and Mackensen, A.: Bipolar seesaw in the northeastern tropical Atlantic during Heinrich stadials, *Geophys. Res. Lett.*, 38, L04706, <https://doi.org/10.1029/2010GL046070>, 2011.
- Ziegler, M., Nürnberg, D., Karas, C., Tiedemann, R., and Lourens, L. J.: Persistent summer expansion of the Atlantic Warm Pool during glacial abrupt cold events, *Nat. Geosci.*, 1, 601–605, <https://doi.org/10.1038/ngeo277>, 2008.